

**STRESS DEPENDENT BEHAVIOUR OF InGaAsP
SEMICONDUCTOR DIODE LASERS**

**STRESS DEPENDENT BEHAVIOUR OF InGaAsP
SEMICONDUCTOR DIODE LASERS**

By

Charles S. Adams, B.A.

A Thesis

Submitted to the School of Graduate Studies

in Partial Fulfilment of the Requirements

for the Degree

Master of Engineering

McMaster University

August 1988

MASTER OF ENGINEERING (1988)
(Engineering Physics)

McMaster University
Hamilton, Ontario

TITLE: **Stress dependent behaviour of InGaAsP**
semiconductor diode lasers.

AUTHOR: **Charles S. Adams, B.A. (Oxford University)**

SUPERVISOR: **Dr. D. T. Cassidy.**

NUMBER OF PAGES: **viii, 77**

ABSTRACT.

The effects of tension and compression applied to unbonded InGaAsP semiconductor diode lasers have been studied. A theoretical calculation of the stress distribution within the laser and an analysis of the effect of strain on optical gain in semiconductors is presented. The observed dependence of threshold, wavelength, and polarization of the laser output on the applied stress is explained in terms of the strain dependence of the valence-band wavefunctions.

The polarization behaviour is found to be related to thermal stress and the structure of the device. A technique has been developed to measure the thermal stress induced by current heating at the 10^5 dynes/cm² level.

The effect of stress on the below threshold behaviour of the lasers was investigated. The results are consistent with the strain dependence of the TE and TM mode gains.

ACKNOWLEDGEMENTS.

The author would like to express his gratitude to Dr. D. T. Cassidy for his advice and encouragement during this work. I would like to thank my mother for her assistance with the figures, Louise Gagnon for stimulating discussions about stress and the Basement people for keeping life interesting.

TABLE OF CONTENTS.

ABSTRACT		iii
ACKNOWLEDGEMENTS		iv
TABLE OF CONTENTS		v
LIST OF ILLUSTRATIONS		vi
CHAPTER 1	INTRODUCTION	1
CHAPTER 2.	EXPERIMENTAL TECHNIQUE.	5
2.1	Introduction.	5
2.2	Thermal properties.	6
2.3	Measurement system.	11
2.4	Method of applying stress.	13
2.5	Summary.	16
CHAPTER 3.	THEORY.	18
3.1	Calculation of stress distribution.	18
3.2	Strain dependence of the valence band wavefunctions.	26
3.3	Summary	32
CHAPTER 4	DISCUSSION OF RESULTS.	33
4.1	Stress dependence of threshold.	33
4.2	Stress dependence of the wavelength.	35
4.3	Effect of contact stress.	37
4.4	Far-field pattern.	41
4.5	Summary.	44
CHAPTER 5.	POLARISATION BEHAVIOUR.	46
5.1	Polarisation resolved <i>LI</i> -curve.	46
5.2	Measurement of thermal stress.	51
5.3	Polarisation of the spontaneous emission.	53
5.4	Summary.	57
CHAPTER 6.	CONCLUSION.	59

APPENDIX A.	LASER DRIVER	63
APPENDIX B.	DATA ACQUISITION	65
APPENDIX C.	<i>LI</i> -CURVE PROGRAM	67
REFERENCES.		74

LIST OF ILLUSTRATIONS.

- 2.1: Oscilloscope trace of a series of light pulses with (a) minimum and (b) maximum applied force.
- 2.2: Change in the thermal decay of the light pulse (Δ) due to the maximum applied force for (a) 200 ns and (b) 500 μ m pulses.
- 2.3: Schematic diagram of the experimental set-up used to produce and detect the light pulses.
- 2.4: Schematic diagram of the apparatus used to produce strain in the laser.
- 2.5: Plot of mass applied to the platform against displacement of the springs. This data is used to calibrate the force applied to the laser.
- 3.1: Schematic diagram showing an exaggerated bending deformation of the laser.
- 3.2: Stress distribution caused by the bending deformation.
- 3.3: Strain-dependence of energy band structure of InGaAsP.
- 4.1: Average relative change in threshold current as a function of the applied stress.
- 4.2: Stress dependence of threshold current for: (a) two stripe geometry DH lasers from the same wafer; and, (b) a PBH laser.
- 4.3: The wavelength corresponding to the maximum gain as a function of the applied stress for a stripe geometry DH laser.
- 4.4: Comparison of the effect of contact and bending stress on threshold.
- 4.5: Effect of contact stress on the maximum output power of a stripe geometry DH laser.
- 4.6: Far-field pattern of a stripe geometry DH laser with no applied stress and $\sigma_x \sim 3 \times 10^9$ dyne/cm².
- 4.7: Polarization resolved far-field pattern of a non-ideal PBH laser.

- 5.1: Polarization resolved LI -curves for (a) a PBH and (b) a stripe geometry DH laser biased with the critical applied stress.
- 5.2: Polarization resolved LI -curve for (a) non-ideal PBH laser and (b) a Q-confining stripe geometry DH laser at the critical applied stress.
- 5.3: Example of the multiple switching observed at a critical applied stress in $\sim 70\%$ of the stripe geometry DH lasers tested.
- 5.4: Current and stress dependence of the TM mode intensity.
- 5.5: Measurement of the thermal stress using the polarization resolved LI -curve at a critical applied stress.
- 5.6: Polarization resolved LI -curve of a PBH laser. Shown here is the saturation of the TM mode at threshold.
- 5.7: The effect of the applied stress on the degree of polarization of (a) a PBH laser and, (b) a stripe geometry DH laser.
- 5.8: Degree of polarization of a reject PBH laser.
- A.1: Circuit diagram of the laser driver.
- B.1: Timing diagram for the measurement system.

CHAPTER 1.
INTRODUCTION.

Strain in the active region of semiconductor diode lasers affects the operating characteristics of the device. For example, uniaxial compressive stress applied perpendicular to the junction plane of the laser increases the threshold current, until a critical strain is exceeded at which point the polarization of the stimulated emission switches from transverse electric (TE) to transverse magnetic (TM). The threshold current decreases with a further increase in strain beyond this critical value [1–6].

Internal strain can be produced at each stage of the fabrication process. For example, stress is induced by the thermal properties of the device. To minimise the dislocation density at the interface, the InGaAsP active is grown lattice matched to the InP layers at the LPE growth temperature (650°C) [7]. As the laser cools to room temperature, a tensile stress is produced in the active layer because the thermal expansion coefficient of InGaAsP is larger than InP [8–10]. Other sources of stress in the active layer include the metallisation process [11] and lattice mismatch [12–14]. In stripe geometry DH lasers the opening of an oxide window has been shown to produce a complex stress distribution which produces photoelastic guiding of the lasing mode [15]. In buried heterostructure lasers, the observation of kinks in the *LI*-curve was attributed to strain in the active layer caused by the etching and regrowth process [16]. Finally, bonding the lasers to a heat-sink produces a threshold change which suggests bonding-induced stress [17]. It is difficult to manufacture a device with a stress free active region therefore stress is a significant parameter in

determining the performance of diode lasers and it is important to understand the strain dependent behaviour.

A useful technique to study the effects of strain on the performance of the laser is to apply a known stress. In this thesis the effect of applied stress on unbonded 1.3 μm InGaAsP/InP laser chips was studied. By using a probe and two point mounting system a bending moment can be induced in the laser. By flipping the chip over it is possible, with this technique, to study the effects of both tension and compression in the same laser. In previous work measurements were performed on lasers bonded to heat-sinks. As a result, strain of only one sign could be investigated.

The effect of both compression and tension on the operating characteristics of InGaAsP semiconductor diode lasers have been studied in more than fifty devices. Three different structures were investigated; stripe geometry planar double heterostructure lasers, planar buried heterostructure lasers (PBH) and stripe geometry planar double heterostructure lasers with a quaternary first-confining layer (*Q-confining*) rather than the conventional InP first-confining layer. The polarisation resolved *LI*-curves at a critical applied stress of each structure were measured and the results are explained in terms of the current-induced thermal stress and the structural differences.

Most of the laser chips examined were rejects. These devices were not suitable for commercial use due to their high threshold, low efficiency or other non-ideal behaviour. These lasers are particularly useful in a study of the effect of strain on device performance because often the non-optimum behaviour is caused by stress within the active region. Understanding why a laser performs poorly is

essential to improving the existing technology.

The effect of strain on the properties of semiconductor diode lasers has been explained in terms of shifts in the valence band quasi-Fermi level [18], changes in the valence band effective masses [19] and a change in the rate of intervalence band absorption [20,21]. However, none of these mechanisms are capable of explaining the observed reduction in threshold as the applied stress is increased above the transition to TM emission. Patel *et al.* [2] calculated the perturbation to the acceptor wavefunction due to a lattice deformation. Their analysis does predict the observed trend in variation of TE and TM thresholds with strain, but is restricted to conduction band to acceptor level type transitions. In the present work, band-to-band transitions are considered and a similar result is obtained. It is shown that the stress dependence of threshold is consistent with a model based on a modification to the valence band wavefunctions due to off-diagonal terms in the strain-dependent Hamiltonian. The mixing of valence band states was first discussed in the work on cyclotron resonance in strained silicon of Hawegawa [22]. This mixing of the valence sub-bands alters the optical matrix elements for transitions between the conduction and valence bands and predicts a stress dependence of the TE and TM mode gains which agrees with the observed threshold changes. The stress dependence of the wavelength of emission is explained in terms of the strain-induced energy band shifts derived from the piezo-electroreflectance work of Pollak *et al.* [23,24]. The results presented in *Chapter 4* are consistent with the shock compression work on GaAs of Lu *et al.* [25] and the photoluminescence work on III-V semiconductors with mismatch strain of Kuo *et al.* [26].

In *Chapter 2*, the thermal properties of InGaAsP semiconductor diode

lasers are considered and it is shown that to avoid threshold changes due to the variation of the thermal impedance between the laser and the heat-sink it is necessary to operate the lasers pulsed. The experimental technique used to produce and detect the light pulses and the method of applying stress is described. The stress distribution due to the bending moment induced by the probe and two point mounting system is calculated in *Section 3.1*. In *Section 3.2*, the effect of the strain on the band structure of III-V semiconductors is discussed and expressions for the stress dependence of the TE and TM mode gains are derived. The results of measurements of the effect of applied stress on threshold, wavelength and the far-field distribution are presented in *Chapter 4*. In *Chapter 5*, thermal stress is discussed and a technique to measure the current-induced thermal stress is reported. Results on the stress dependence of the degree of polarisation of the spontaneous emission are considered in *Section 5.3*. In *Chapter 6* a summary of the results and suggestions for further work are presented.

This work is to be published as "Effects of stress on threshold, wavelength and the polarization of the output of InGaAsP semiconductor diode lasers" by C.S. Adams and D.T. Cassidy in the *Journal of Applied Physics*.

CHAPTER 2.

EXPERIMENTAL TECHNIQUE.

2.1 Introduction.

Useful information about the physics of operation of semiconductor diode lasers is obtained from measurement and analysis of the dependence of threshold current on applied stress. Threshold also depends on temperature, therefore to investigate the effects of stress it is important to operate the laser at a constant temperature. A steady-state (to within $\pm 0.1^{\circ}\text{C}$) laser heat-sink temperature can be obtained with a thermoelectric cooler and electrical feedback circuit. However, as soon as current is injected into the device there is a temperature increase in the active region of the laser due to non-radiative recombination and Joule heating. The rate at which the active temperature increases is described by a characteristic time constant which depends on the thermal impedance between the laser and the heat-sink and the heat capacities. Experimentally, it has been demonstrated that there are two time constants [27]; one of a few hundred nanoseconds, for the laser to reach equilibrium with itself, and one of a few microseconds, for the laser to reach equilibrium with the heat-sink. The second time constant depends on the thermal impedance between the laser and the heat-sink. For bonded lasers, the thermal impedance is a constant and does not usually concern the experimenter. However, in this work unbonded laser chips were used and the thermal impedance is sensitive to the force applied to produce a stress in the device. This means that the steady-state temperature difference between the active region and the heat-sink depends on the

applied force. If the force is small, poor thermal contact is achieved and there is a large temperature increase in the active region. This temperature increase causes an increase in the lasing threshold. It follows that if the lasers are operated d.c., a stress dependence of threshold due to the variation of the thermal impedance will be observed.

In this work the stress dependence of threshold due to mechanisms other than thermal will be studied. Therefore, it is important that the effect of the thermal impedance be minimised. This is achieved by operating the laser with short current pulses and a low duty-cycle. To establish how short and how low, it is necessary to look at the thermal properties of semiconductor diode lasers in more detail.

2.2 Thermal properties of InGaAsP semiconductor diode lasers.

The threshold current of semiconductor diode lasers depends on temperature. If a current pulse is injected into the device the heat generated causes an increase in threshold and consequently a decrease in the light output. The light output decreases with time until the laser temperature attains a steady-state. The variation of the output power due to current heating is known as the *thermal decay*. Both the shape of the thermal decay and the total power decrease between the time of the current step and steady-state depend on the thermal impedance between the laser and the heat-sink. Therefore by adjusting the applied force the thermal decay is altered. This is illustrated in Fig. 2.1. Normally the thermal impedance is large and the current-induced heating causes a large temperature rise in the active region. As a result, threshold increases dramatically and the lasing is extinguished after a few

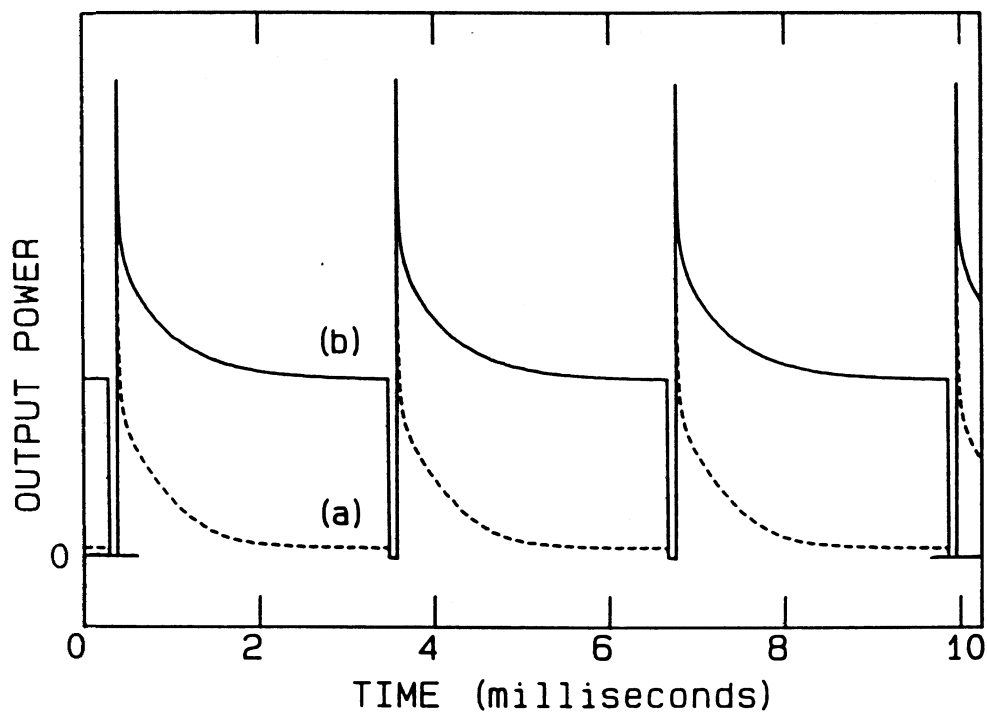


Figure 2.1: Oscilloscope trace of a series of light pulses with (a) minimum and (b) maximum applied force. For the maximum applied force, the thermal impedance between the laser and the heat-sink is sufficiently low for c.w. operation of the laser.

milliseconds. This is shown in Fig. 2.1(a). Now if a large force is applied to the laser, so that the thermal impedance is reduced, then the temperature rise in the active region is smaller and c.w. operation is achieved, as shown in Fig. 2.1(b). These results show that the applied force has a large effect on the steady-state temperature and consequently on the c.w. output of the laser. However, near the beginning of the pulse there is little heating. The magnitude of the threshold change, due to a change in the thermal impedance caused by adjusting the applied force, increases from zero at the beginning of the pulse to a maximum at steady-state. It follows that if we make our measurements sufficiently soon after the start of the each pulse, then the thermal impedance effect can be neglected. The time scale involved is determined by comparing the thermal decays with the laser under maximum and minimum applied force.

Using equations which describe the effects of heating on semiconductor diode lasers an expression for the thermal decay can be derived. The temperature dependence of threshold is given by the empirical relationship [28]

$$I_{th}(T) = I_{th}(T') \exp \left(\frac{T-T'}{T_0} \right) \quad (2.1)$$

where T and T' are the temperatures of the active region and the heat-sink respectively, $I_{th}(T)$ is the threshold current at a temperature T and T_0 is a characteristic temperature which for InGaAsP lasers is $\sim 50 - 70$ K [29]. The output power of the laser $P(I, T)$ above threshold can be written as

$$P(I, T) = \eta [I - I_{th}(T)] \quad (2.2)$$

where I is the current and η is the efficiency. Substituting for $I_{th}(T)$ in equation (2.2) one finds that

$$P(I, T) = \eta [I - I_{th}(T') \exp(\frac{T - T'}{T_0})] . \quad (2.3)$$

For simplicity it is assumed that there is only one time constant τ . The absolute temperature rise $\Delta T(t) = T - T'$, of the active region, at a time t after the start of the pulse is given by [29]

$$\Delta T(t) = \Delta T_f [1 - \exp(-t/\tau)] \quad (2.4)$$

where ΔT_f is the steady state temperature difference between the active region and the heat-sink. Substituting for $T - T'$ in equation (2.3) an expression for $P(I, t)$ is found:

$$P(I, t) = \eta \left[I - I_{th}(T') \left[\exp \Delta T_f (1 - \exp(-t/\tau)) / T_0 \right] \right] . \quad (2.5)$$

Thus, the decrease in the output power after a time t can be written as,

$$\Delta P(I, t) = -\eta I_{th}(T') \left[\exp[\Delta T_f (1 - e^{-t/\tau}) / T_0] - 1 \right] . \quad (2.6)$$

The temperature difference ΔT_f is usually a few degrees. Therefore, $\Delta T_f / T_0$ is small and equation (2.6) can be expanded in a Taylor series. Neglecting

terms of second order and higher

$$\Delta P(I,t) = -\frac{\eta I_{th}(T') \Delta T_f}{T_o} \left[1 - \exp(-t/\tau) \right]. \quad (2.7)$$

Hence the thermal decay is approximately exponential in time. Both the steady-state temperature difference ΔT_f and the time constant τ depend on the thermal impedance between the laser and the heat-sink.

The effect of the applied force on the thermal decay was determined experimentally by recording the light pulse shape using a digital oscilloscope (LeCroy 9400). The results are shown in Fig. 2.2. It is apparent from the initial pulse amplitude (inset of Fig. 2.2(b)), that threshold depends on the applied force through the strain dependence of the gain. As the thermal decay, ΔP , given by equation (2.7) also depends on threshold, it is necessary to compare ΔP_1 and $\Delta P_2 I_{th1}/I_{th2}$ where $\Delta P_{1,2}$ and $I_{th1,2}$ are the thermal decays and the values of threshold at the heat-sink temperature with minimum and maximum applied force respectively. The magnitude of the effect of the thermal impedance is described in terms of the quantity $\Delta = [\Delta P_1 - \Delta P_2 I_{th1}/I_{th2}]/P_1$, where P_1 is the amplitude of the light pulse at time t . If the applied force has no effect on the thermal impedance then Δ would be zero at all times. It is apparent from Fig. 2.2 that Δ is not zero but increases with the duration of the pulse. For the 500 μ s pulse shown in Fig. 2.2(a), the thermal decay is approximately exponential in time, as expected from equation (2.7). After 200 μ s, the difference in the output power caused by changing the applied force is given by $\Delta \sim 11\%$.

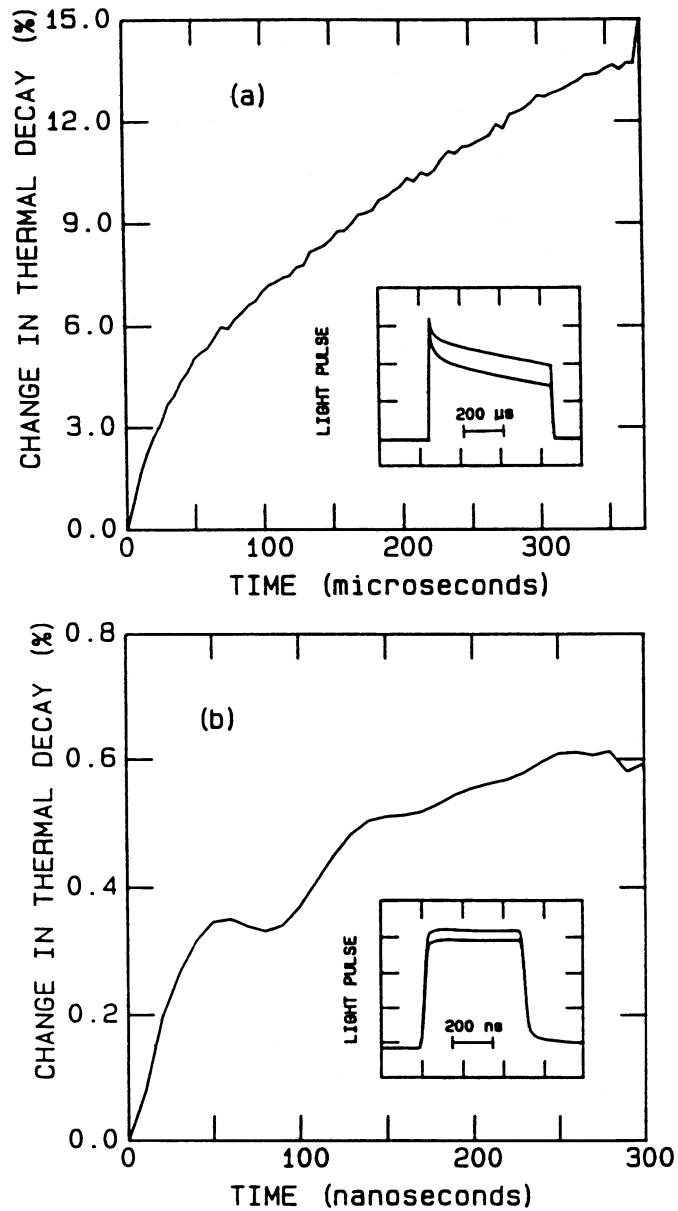


Figure 2.2:

Change in the thermal decay of the light pulse (Δ), due to the maximum applied force. The thermal decay for (a) 500 μ s and (b) 500 ns pulses are shown. Inset, the complete light pulses which are used to calculate Δ .

For $t < \tau$ equation (2.7) reduces to

$$\Delta P(I,t) = - \frac{\eta I_{th}(T) \Delta T_f}{\tau T_0} t \quad (2.8)$$

i.e., the thermal decay is linear. However, for the 500 ns pulse shown in Fig. 2.2(b) the thermal decay appears exponential which may be explained in two ways. One possibility is that exponential decay results from the faster time constant ($\tau \sim 100$ ns) required for the laser to thermalise with itself [27]. Alternatively the relatively large change in the thermal decay in the initial 50 ns of the pulse may be caused by an uncertainty in the initial pulse amplitude due to ringing on the current pulse.

The important point to make about the results shown in Fig. 2.2(b) is that during the first 200ns of the pulse, the change in the thermal decay due to the maximum applied force, *i.e.* $\Delta P_1 - \Delta P_2 I_{th1} / I_{th2}$, is less than 0.5% of the pulse amplitude ($\Delta < 0.5\%$). The change in the pulse amplitude at $t = 0$, due to the same applied force is - 10%. This means that, if the measurement system is designed to record data within 200ns of the beginning of each pulse, then the effect of the thermal impedance on threshold is more than twenty times smaller than the effect of the stress induced in the active region. Both effects scale with the applied force. Thus, using 200ns pulses is a satisfactory operating condition for the experiments.

The duty-cycle required to avoid steady-state heating of the chip was determined by the following method. The pulse length was set to 200ns, then the duty-cycle was increased until a measurable decrease (1%) in the output power was observed. This occurred when the duty-cycle was increased above a few percent.

Thus, for a duty-cycle $< 0.1\%$ the heat generated by each current pulse dissipates before the next pulse arrives. In this case, the steady-state temperature of the active region is essentially equal to the heat-sink temperature, which is independent of the applied force.

In conclusion, the results of the thermal measurements show that by operating the laser with current pulses 200ns in length at a duty-cycle of 0.1%, the effects of the thermal impedance between the laser and the heat-sink can be neglected.

2.3 Measurement system.

It has been established that to avoid thermal effects which depend on the applied force the laser must be operated with short current pulses and a low duty-cycle. A schematic diagram of the experimental set-up used to produce and detect the light pulses is provided in Fig.2.3. The current pulses are supplied by the laser driver which consists of a constant current source and a differential pair arrangement. The pulse length and the duty-cycle are controlled by the input of TTL pulses from a pulse generator (Wavetek 802). For a 200 ns pulse with an amplitude of 150 mA, after the first 50 ns the current remains constant to within ± 1 mA. The amplitude of the current pulse is set by the voltage V_{in} , which is provided by the digital acquisition system (TransEra MDAS 7000). This enables the current to be controlled directly by a computer. A more detailed discussion of the laser driver circuit is presented in Appendix A.

The laser beam was collimated using a microscope objective (Numerical

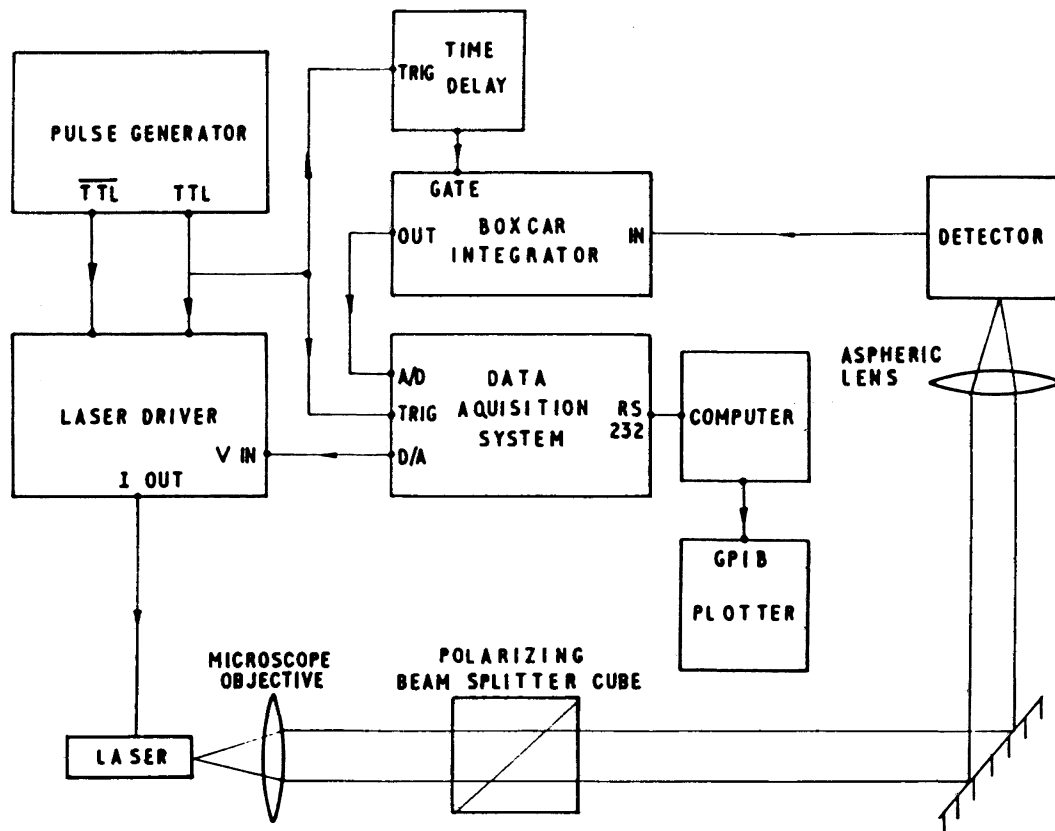


Figure 2.3: Schematic diagram of the experimental set-up used to produce and detect the light pulses.

Aperture = 0.35, Magnification = 18x) and focused onto the detector using an aspheric lens (Focal length = 18mm, Diam. = 24mm). A polarising beam splitter cube (Newport model 10FC16PB.9) was placed in the path of the collimated beam to determine the polarization state of the laser emission.

To detect the light output, an InGaAs p-i-n photodiode (Epitaxx ETX 300) with an active area 300 μm in diameter was used. It is easier to work with larger area detectors, but with increasing area there is a loss of speed. The ETX300 is sufficiently fast to follow the light pulse and has an active area which is convenient to work with. The detector is connected reversed biased in series with a 50 Ω resistor to a 6 V supply. The output, measured across the resistor, is digitised and stored in the computer. The input bandwidth of the sample-and-hold circuit in the data acquisition system is 1 MHz. Therefore, to make a measurement on a pulse which only lasts 200ns, a boxcar integrator (Evans Electronics 4130A) was used. While the gate is open, the boxcar integrates the difference between the input and the output. Hence, after a total integration time of a few RC time constants, the output is essentially equal to the input. The gate is controlled by a programmable time delay circuit (Evans Electronics 4141). This allows both the integration time and the time of the measurement after the beginning of each pulse to be controlled. The output of the boxcar is stored while the gate is closed. The data acquisition system is triggered to measure the voltage on the boxcar during the 1 ms time interval between successive pulses. These values are digitised, averaged and the average is sent to the computer. The operation of the boxcar integrator and the data acquisition system is discussed further in *Appendix B*.

The current passing through the laser can be measured directly from the

driver circuit, or can be calculated from the input voltage V_{in} (see *Appendix A*). If the current and the output power are known, an LI -curve can be plotted. The threshold current is calculated from the LI -curve. A computer program which records the LI -curve and calculates threshold is listed in *Appendix C*. The required current values are output from a buffer within the data acquisition system. An averaged measurement of the light intensity is made at each current. A typical LI -curve contains one hundred points. The threshold current is determined by performing a straight line fit on the data points which fall between two specified light levels (say 0.2 – 2.0 mW). Threshold is given by the intersection of this line and the current axis.

A repeated measurement of threshold provides an indication of the accuracy and reproducibility of the laser driver and the detection system. The threshold current of the same stripe geometry DH laser was measured twenty-one times. The averaged value of threshold was $I_{th} = 99.6 \pm 0.2$ mA, where the error is equal to two standard deviations. The change in threshold due to the external stresses applied in this work are $\leq 15\%$. Therefore, the error associated with experimental set-up is small compared to the effects which are being studied.

2.4 Method of applying stress.

The unbonded laser chips are supported across two diamonds, which are in thermal contact with the heat-sink as shown in Fig. 2.4. The laser chips are placed on the diamonds using a micropositioner and a vacuum probe. The heat-sink is clamped firmly, such that when a stress is applied the support does not move and

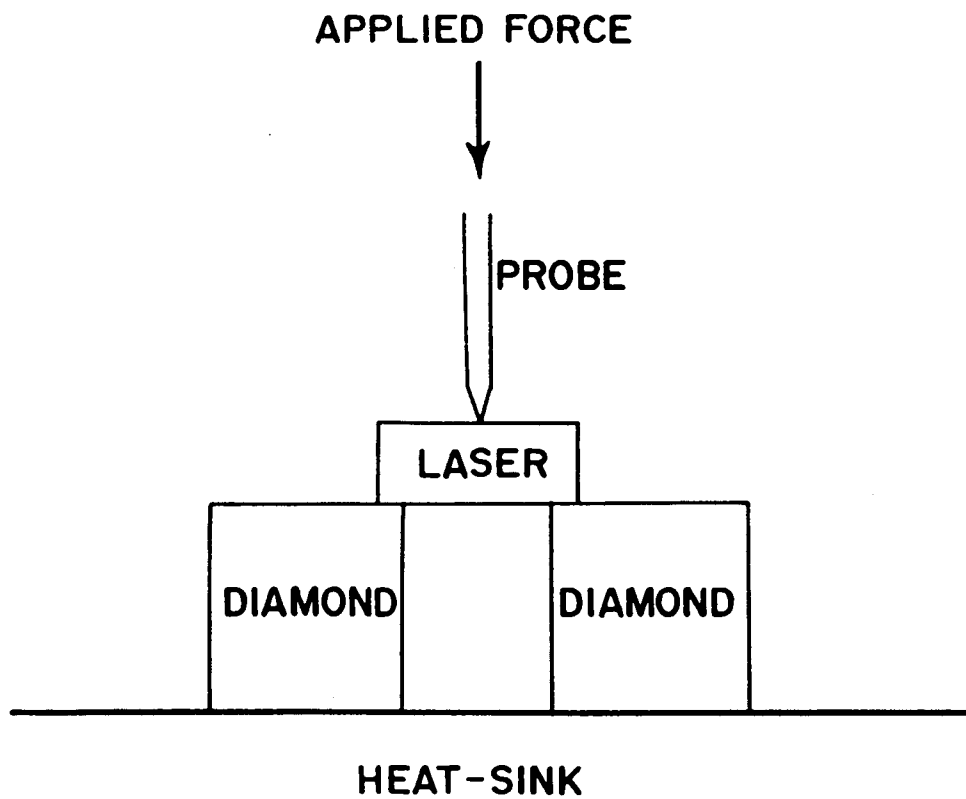


Figure 2.4:

Schematic diagram of the apparatus used to produce strain in the laser.

affect the optical alignment. The diamonds form one electrical contact to the laser. A stress is applied through the metal probe shown in Fig. 2.4. The probe is also the other electrical contact. The connections to the probe and the diamonds can be reversed so that the laser can be positioned with the *p-side* either up or down. The laser driver switches upto 230mA through the laser in a few nanoseconds, therefore it was important to minimise the volume of conducting metal in the probe and mount, to avoid large capacitances which slow down the rise time and create ringing on the pulse.

The probe has a uniform cross-section along the length of the laser (*y-axis*). This loading distribution in conjunction with the two point mounting system results in a bending of the lattice. The stress distribution due to the bending has been derived using the mechanics of solids. This calculation is reported in *Section 3.1*. As well as the bending stress there is a deformation below the probe caused by the contact. A theoretical calculation of the stress induced at the contact of two elastic bodies was first attempted by Hertz. It has been shown that these *Hertzian stresses* decay exponentially with distance away from the contact region [30]. The characteristic length of the decay is approximately equal to the width of the contact area. In our experiments, we are only interested in the stress in the active region of the laser. The contact width is $\sim 10 - 20 \mu\text{m}$, therefore if the probe is $\geq 20 \mu\text{m}$ from the active region the Hertzian stresses are negligible. The active region is $\sim 5 \mu\text{m}$ wide and $\sim 2 \mu\text{m}$ from the *p-side*. The height of the wafer is $\sim 100 \mu\text{m}$. Thus, with the laser positioned with the *active region down*, the applied stress is given accurately by the bending calculation. However, with the *active region up* the Hertzian stress will be important if the probe is positioned close to the stripe. The

magnitude of the contact stress depends on the exact profile of the probe which is difficult to determine experimentally. To be able to make comparisons between the *active region up* and the *active region down* measurements it is convenient to study the active region up behaviour such that the Hertzian stresses can be neglected. This is achieved by placing the probe $\sim 20 \mu\text{m}$ to one side of the stripe.

The influence of the contact stress on threshold was studied experimentally (see *Section 4.3*). It was found that the contact produced an increase in threshold, whereas the bending stress (active region up) causes threshold to decrease. This difference allows us to confirm experimentally that the Hertzian stress becomes negligible if the probe is moved more than one characteristic length away from the stripe.

The Hertzian stress distribution becomes more localised if a sharper probe is used [30]. However, it was found that a sharper probe caused the laser to cleave at a much lower applied force.

The profile of the probe was obtained using a brass polishing technique. A piece of brass, with a hole for the probe, was shaped to the desired profile. The probe was inserted in the brass and polished down to the same profile. This technique is necessary to produce a probe which provides a uniform load along the length of the laser.

The force applied to the probe must be known to calculate the stress distribution. The applied force was calibrated using the spring loaded mount which supports the probe. The probe is attached to a platform, which is loaded with lead weights. This platform rests on springs which are held in place by an aluminum bar. The bar is free to move in the vertical direction. By moving the bar up and down,

the weight of the platform is transferred from the laser to the bar and vice versa. The position of the bar and hence the force applied to the laser is controlled by a micropositioner.

By loading the platform with a known mass and measuring the displacement, the spring constant can be determined. To measure the displacement the position of the bar is adjusted until the platform is returned to its original position. The displacement is the distance the bar has been moved, which can be read directly off the micropositioner. A plot of mass against displacement is shown in Fig. 2.5. The experiment was repeated twice, for both increasing and decreasing micrometer position, to determine whether friction between the platform and the bar has any effect on the force. The results show that friction is not important. A straight line fit through 80 data points gives a value for the spring constant of $k = 0.79 \pm 0.02$ N/mm. As the displacement of the micrometer is known the applied force can be calculated.

The experimental results on thermal stress (see *Section 5.2*) show that stresses as small as 10^5 dyne/cm² can be accurately reproduced with this technique. The lasers tend to break or become permanently damaged if the applied force, $F \geq 3$ N. For this reason, the maximum force which can be applied was limited to this value.

2.5 Summary.

In this chapter the thermal properties of InGaAsP semiconductor diode lasers were considered. It was found that to neglect variations in the thermal

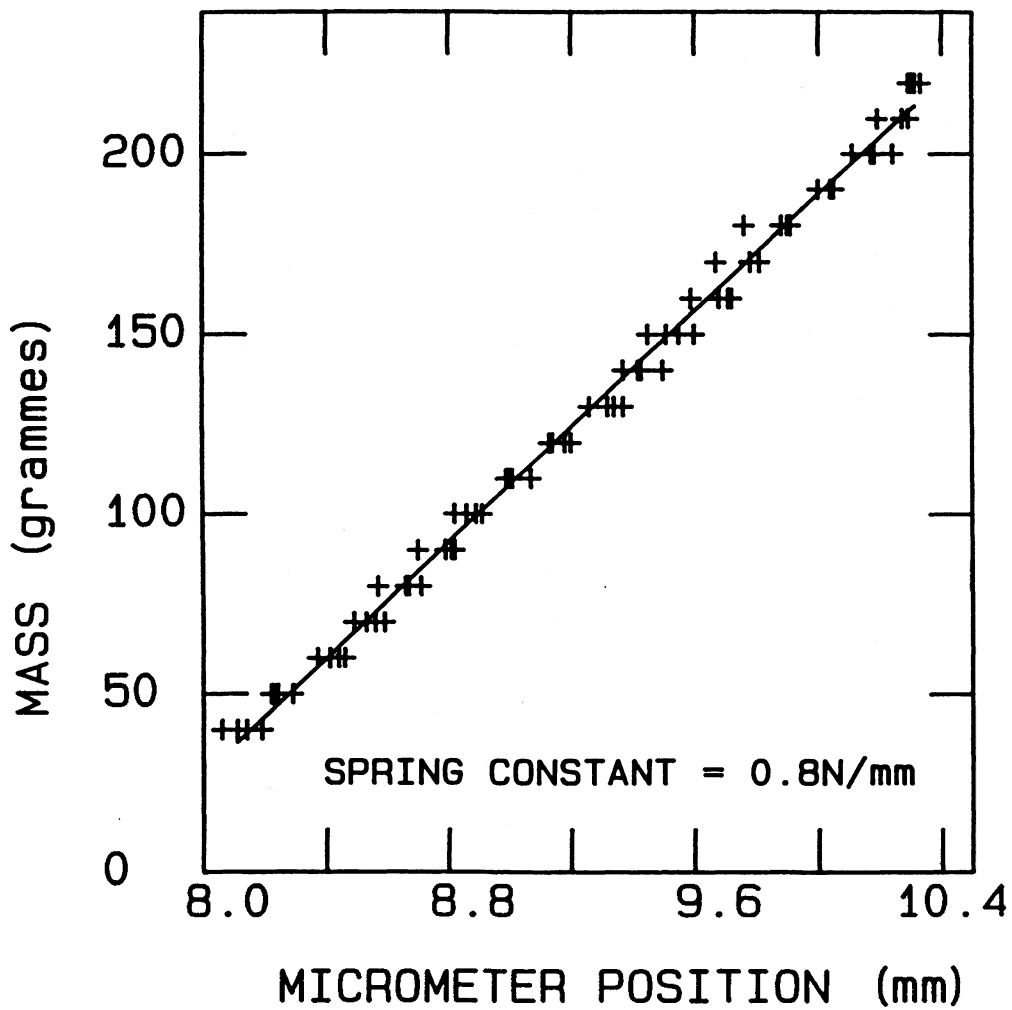


Figure 2.5:

Plot of mass applied to the platform against displacement of the springs. This data is used to calibrate the force applied to the laser.

impedance between the laser and the heat-sink, it is necessary to operate the laser with 200 ns pulses and a duty-cycle of $\leq 0.1\%$. The laser driver used to produce the current pulses and the measurement system used to detect the light output was discussed in *Section 2.3*. The method of applying stress and a technique to calibrate the applied force was presented in *Section 2.4*. In the next chapter the stress distribution which results from this technique of applying stress will be calculated.

CHAPTER 3.

THEORY.

3.1 Calculation of stress distribution.

If a force is applied to a solid, the deformation can be described in terms of stresses and strains. For a three dimensional problem the stress and strain are second-rank tensors. The stress is written as σ_{ij} , where $\sigma_{ij} dS$ is the force in the i -direction exerted by material on the j -side of the element of area dS . The strain components can be expressed in terms of the stress as follows [31]

$$\epsilon_{ij} = S_{ijkl} \sigma_{kl} \quad (3.1)$$

where S_{ijkl} is the compliance tensor. Equation (3.1) is equivalent to *Hooke's law*. By symmetry it follows that $\epsilon_{ij} = \epsilon_{ji}$ and $\sigma_{ij} = \sigma_{ji}$, therefore the nine independent stress/strain components can be reduced to six. The suffices can be replaced by a single suffix m , such that equation (3.1) becomes,

$$\epsilon_m = S_{mn} \sigma_n \quad (3.2)$$

The number of independent non-zero components in the compliance tensor is further reduced by rotation and inversion symmetry. The laser is made of InP and InGaAsP which both have a zinc-blende structure. In this case there are only three independent compliance components. Equation (3.2) becomes

$$\begin{bmatrix} \epsilon_1 \\ \epsilon_2 \\ \epsilon_3 \\ \epsilon_4 \\ \epsilon_5 \\ \epsilon_6 \end{bmatrix} = \begin{bmatrix} S_{11} & S_{12} & S_{12} & 0 & 0 & 0 \\ S_{12} & S_{11} & S_{12} & 0 & 0 & 0 \\ S_{12} & S_{12} & S_{11} & 0 & 0 & 0 \\ 0 & 0 & 0 & S_{44} & 0 & 0 \\ 0 & 0 & 0 & 0 & S_{44} & 0 \\ 0 & 0 & 0 & 0 & 0 & S_{44} \end{bmatrix} \begin{bmatrix} \sigma_1 \\ \sigma_2 \\ \sigma_3 \\ \sigma_4 \\ \sigma_5 \\ \sigma_6 \end{bmatrix}. \quad (3.3)$$

The compliances can be written in terms of Young's Modulus E , Poisson's ratio ν , and the Bulk Modulus G as follows

$$S_{11} = \frac{1}{E} \quad (3.4)$$

$$S_{12} = \frac{-\nu}{E} \quad (3.5)$$

$$S_{44} = \frac{1}{G}. \quad (3.6)$$

Thus, the equations for the normal components of strain are

$$\epsilon_x = \frac{1}{E} [\sigma_x - \nu(\sigma_y + \sigma_z)] \quad (3.7)$$

$$\epsilon_y = \frac{1}{E} [\sigma_y - \nu(\sigma_x + \sigma_z)] \quad (3.8)$$

$$\epsilon_z = \frac{1}{E} [\sigma_z - \nu(\sigma_x + \sigma_y)]. \quad (3.9)$$

These equations are the starting point for calculating the stress distribution within the laser.

The lasers are placed on two diamonds and a load is applied in the middle

of the top surface. This configuration produces a cylindrical deformation of the lattice [32]. The stress distribution in the laser consists of a superposition of the stress resulting from the induced bending and the Hertzian stresses close to the contact point. A measurement technique was adopted such that the Hertzian stresses within the active region are negligible. In this section, an expression for the bending stress will be derived. The cylindrical deformation is illustrated in Fig. 3.1. It is convenient to define a coordinate system with the origin at the centre of the laser structure. The diamonds supports are located at $x = \pm l$. The active region is centred at $x = 0$, $z \sim \pm h/2$, where the plus and minus signs refer to the *active region up* and *active region down* situations respectively. It is assumed, that the mechanical properties of the laser are homogeneous and that the loading is uniform in the y -direction (*i.e.*, along the length of the laser cavity). As there is no constraint in the y -direction, $\sigma_y \sim 0$ [33].

Consider the region close to the z -axis, *i.e.*, away from the supports. The boundary condition for the vertical component of stress on the bottom surface of the laser is given by [32]

$$\sigma_z \Big|_{z=-\frac{h}{2}} = 0 . \quad (3.10)$$

The boundary condition on the top surface is

$$\sigma_z \Big|_{z=\frac{h}{2}} = q(x) \quad (3.11)$$

where $q(x)$ is the load distribution function. Using these boundary conditions an

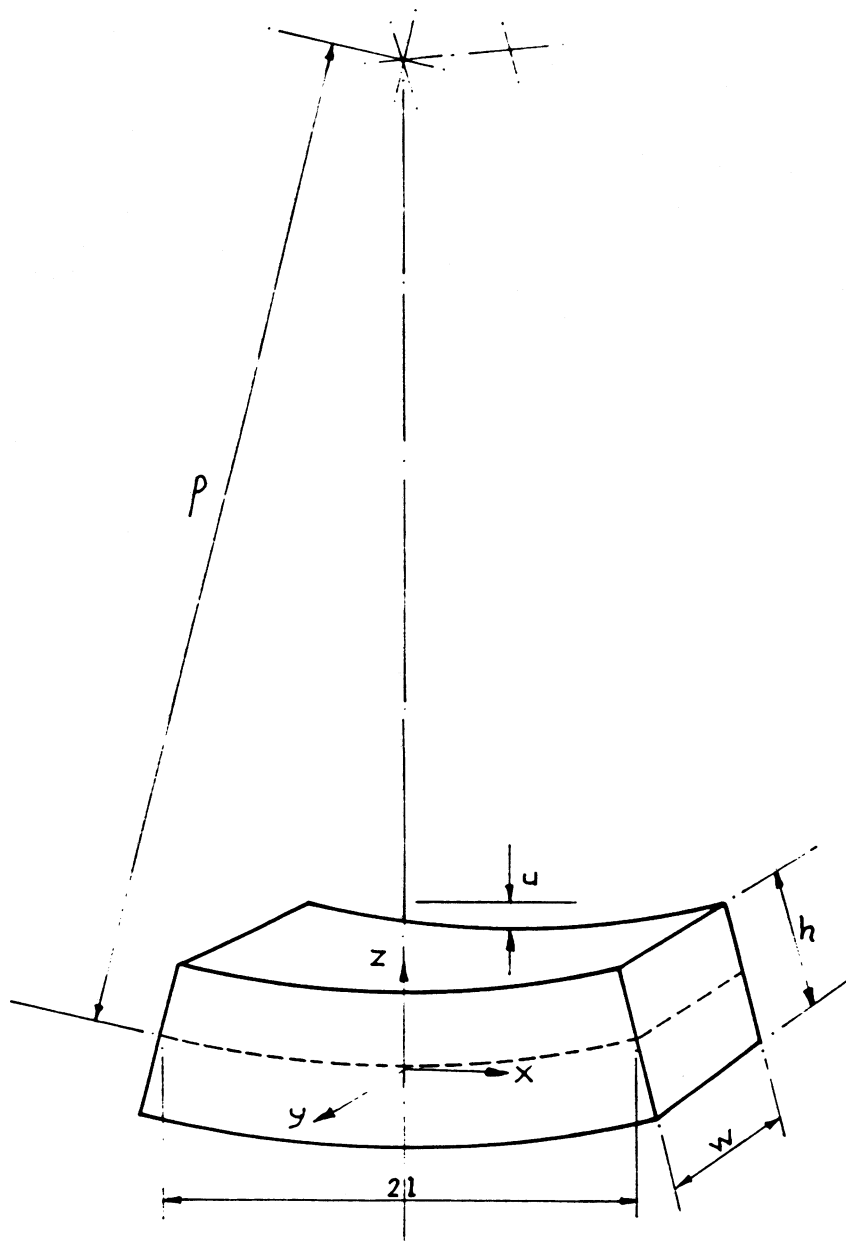


Figure 3.1:

Schematic diagram showing an exaggerated bending deformation of the laser. The coordinate system used in the calculation of the bending stress is shown.

expression for the vertical component of stress can be derived [32]

$$\sigma_z(x, z) = \left[2 \left(\frac{z}{h} \right)^3 - \frac{3}{2} \frac{z}{h} - \frac{1}{2} \right] q(x). \quad (3.12)$$

It follows from equation (3.12) that σ_z is small outside the contact region. In this calculation the contact stress will be ignored therefore $\sigma_y = \sigma_z = 0$ and equation (3.9) reduces to

$$\epsilon_x = \frac{\sigma_x}{E}. \quad (3.13)$$

By symmetry, the strain and hence the stress is zero on the surface which bisects the structure in the horizontal plane. This surface is known as the *center plane*. Consider a surface parallel to the center plane, but a distance z above or below. The elongation of this surface in the x -direction is $2lz/\rho$, where ρ is the radius of curvature of the center plane and $2l$ is the width of the laser. The strain is equal to the ratio of the extension to the original length. Thus, the x -component of strain is given by

$$\epsilon_x = \frac{z}{\rho} \quad (3.14)$$

and therefore the stress can be written as

$$\sigma_x = \frac{Ez}{\rho}. \quad (3.15)$$

The radius of curvature, ρ , is a function of x . To find this x -dependence, ρ is written in terms of the bending moment M and then the bending moment is derived by applying the boundary conditions underneath the probe and at the supports. The bending moment, can be written as

$$M = \int_{-\frac{w}{2}}^{\frac{w}{2}} \int_{-\frac{h}{2}}^{\frac{h}{2}} \sigma_x z \, dz dy \quad (3.16)$$

where w is the width and h is the thickness of the laser. Substituting for σ_x and evaluating the integral one obtains

$$M = \frac{Ewh^3}{12\rho} . \quad (3.17)$$

Substituting for ρ in equation (3.15) using equation (3.17) it follows that

$$\sigma_x = \frac{12M}{wh^3} z . \quad (3.18)$$

The rate of change of the bending moment with distance, is equal to the shear force V and the rate of change of the shear force is equal to the load distribution $q(x)$ [33]. These relationships may be written as

$$\frac{dM(x)}{dx} = V(x) \quad (3.19)$$

$$\frac{dV(x)}{dx} = q(x) . \quad (3.20)$$

By integrating equations (3.19) and (3.20), an expression for $M(x)$ and hence for $\sigma_x(x,z)$ is obtained. This calculation requires a knowledge of the load distribution function $q(x)$. The exact form of the load distribution is unknown. However, this function does not significantly effect the results of this calculation. For simplicity, it is assumed that the load is applied over a region with a lateral dimension of $2a$, and is described by the parabolic function,

$$q(x) = \begin{cases} \frac{3F}{4wa} \left(1 - \frac{x^2}{a^2}\right) & |x| < a \\ 0 & a < |x| < l . \end{cases} \quad (3.21)$$

Experimentally, the distance, $2a$ was determined by measuring the footprint of the probe in the gold metallisation on the surface of the laser ($2a - 20 \mu\text{m}$).

To integrate equations (3.19) and (3.20) using this expression for $q(x)$ it is helpful to divide the x -axis into three regions:

Region 1: $-l < x < -a$.

In this region the load distribution is zero. The boundary conditions are:

- (i) By symmetry, the shear force at one support must be equal to one half of the total applied force F , *i.e.*, $V(-l) = \frac{F}{2}$.
- (ii) The bending moment at the support must be zero, *i.e.*, $M(-l) = 0$.

Thus, the bending moment is given by

$$M(x) = \frac{F}{2} (l+x). \quad (3.22)$$

Region 2: $-a < x < a$.

In this case, $q(x) \neq 0$ and the boundary condition are:

(i) By symmetry, $M(-x) = M(x)$.

(ii) The bending moment must be continuous, i.e., $M(-a) = M(a)$.

This gives,

$$M(x) = \frac{F}{2} \left[\left(l - \frac{3}{8}a \right) - \frac{3x^2}{4a} \left(1 - \frac{x^2}{6a^2} \right) \right]. \quad (3.23)$$

Region 3: $a < x < l$.

This is the same as *Region 1*, except for the sign of x . Therefore

$$M(x) = \frac{F}{2} (l-x). \quad (3.24)$$

Combining the expressions for each region, the bending moment is given by

$$M(x) = \begin{cases} \frac{F}{2} \left[\left(l - \frac{3}{8}a \right) - \frac{3x^2}{4a} \left(1 - \frac{x^2}{6a^2} \right) \right] & |x| < a \\ \frac{F}{2} (l - |x|) & a < |x| < l. \end{cases} \quad (3.25)$$

Substituting for $M(x)$ in equation (3.18) an expression for the x -component of stress is obtained

$$\sigma_x(x,z) = \begin{cases} \frac{6F}{wh^3} \left[\left(l - \frac{3}{8}a \right) - \frac{3x^2}{4a} \left(1 - \frac{x^2}{6a^2} \right) \right] z & |x| < a \\ \frac{6F}{wh^3} (l - |x|) z & a < |x| < l \end{cases} \quad (3.26)$$

Contours of constant σ_x in the x - z plane (*i.e.*, looking at the laser facet) are shown in Fig. 3.2. It is important to note that in this experiment the deformation is parallel to the junction plane whereas in all previous work [1-6] the applied stress was perpendicular to the junction plane. This difference is significant, because the direction of the deformation determines the polarization of light emitted from optical transitions involving different valence band states (see *Section 3.2*).

An alternative calculation of the stress distribution for the same problem has been reported by Love [34]. He considered a solid bar supported across two rollers and deformed by a force applied to a third roller on the top surface. The dominant terms in his expression are the same as in equation (3.26).

The operating characteristics of the laser are determined by the material properties within the active region. Therefore we are only interested in the magnitude of the applied stress at this location. As the active region is small, *i.e.*, the width is less than the contact width a , it follows from equation (3.26) that there is a negligible variation of stress across the active area. Using the following dimensions; $w = 200 \mu\text{m}$, $h = 100 \mu\text{m}$, $l = 150 \mu\text{m}$ and $a = 10 \mu\text{m}$, the stress within the active region ($x = 0$, $z = \pm 50 \mu\text{m}$) is given by equation (3.26)

$$\sigma_x = \pm 1.4 \times 10^9 F \text{ (dyne/cm}^2\text{)} \quad (3.27)$$

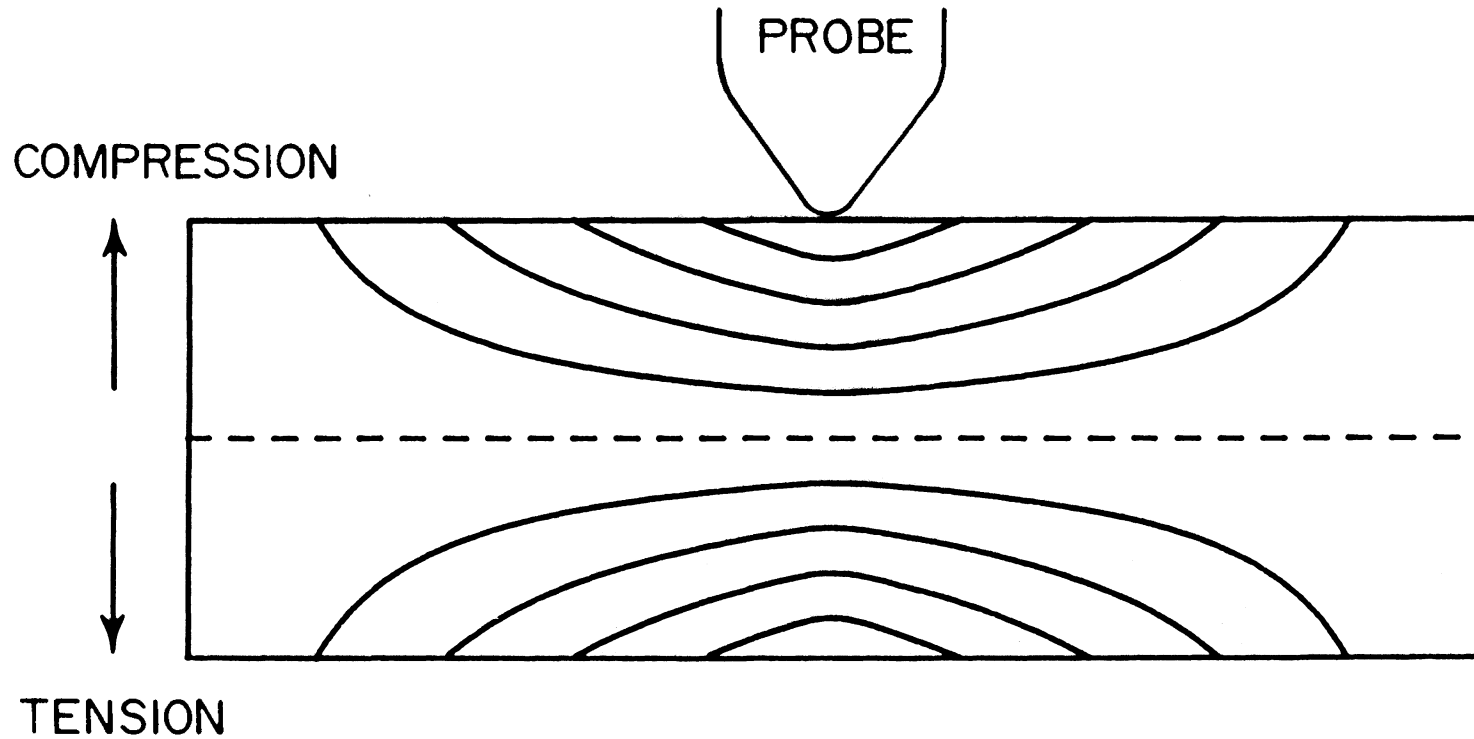


Figure 3.2:

Stress distribution caused by the bending deformation. Shown here are lines of constant stress in the $x-z$ plane, *i.e.*, parallel to the laser facet. The dotted line corresponds to the centre plane, where the stress is zero. Above the centre plane, the stress is compressive and below the centre plane, it is tensile.

where F is the applied force in Newtons. The stress in the active region is compressive ($\sigma_x < 0$), when the laser is positioned with the *active region up* and tensile ($\sigma_x > 0$), when the laser is positioned with the *active region down*.

Experimentally, it was found that the laser would cleave if the applied force exceeded about 3N. Therefore, the effects of tensile and compressive stress up to $\sim 4 \times 10^9$ dyne/cm² could be studied without damaging the laser.

3.2 Strain dependence of the band structure of InGaAsP.

To understand why the threshold current, or wavelength of emission of a diode laser change when a stress is applied it is necessary to examine the effect of strain on the band structure of the semiconductor. The band structure of InGaAsP is similar to other III–V materials with a zinc–blende structure [35]. The conduction band is *s-like* and two fold degenerate due to the electron spin. The valence band is *p-like*, consisting of a $P_{3/2}$ multiplet and a $P_{1/2}$ level known as the split-off band, because it is shifted below the valence band maximum by the spin-orbit interaction. For InGaAsP fabricated for laser emission at 1.3 μm the magnitude of the spin-orbit splitting Δ at room temperature is ~ 250 meV [36]. The $P_{3/2}$ multiplet is composed of a heavy-hole band (with angular momentum along the quantization axis $|M_J| = \pm 3/2$) and a light-hole band (with angular momentum component $|M_J| = \pm 1/2$). Each valence band is two fold degenerate due to the electron spin. For a perfect crystal the light- and heavy-hole bands are essentially degenerate near zone centre. A deformation of the lattice reduces the symmetry and results in a lifting of this degeneracy. The energy shifts of the light- and heavy-hole bands

relative to the conduction band due to a uniaxial deformation along a [100] direction are [24],

$$\Delta E_{hh} = 6 \sigma_x \text{ (meV)} \quad (3.28)$$

$$\Delta E_{lh} = 1.2 \sigma_x \text{ (meV)} \quad (3.29)$$

respectively, where σ_x is the applied stress ($\times 10^9$ dyne/cm²). For a compressive strain, the bandgap increases and the heavy-hole band moves below the light-hole band. For a tensile strain, the bandgap decreases and the heavy-hole band moves above the light-hole band. The energy band shifts, under tension and compression, are illustrated in Fig. 3.3.

The natural cleavage plane of III-V semiconductor is a {110} plane. Thus, the deformation induced by bending the laser is parallel to the [110] direction. If stress is applied in the [100] or [111] direction, then by choosing the quantization axis parallel to the stress direction, the strain-Hamiltonian commutes with the angular momentum operator and M_J is a good quantum number [22]. However, for a [110] stress M_J is not, in general, a good quantum number. In this case, the strain-split levels consist of mixtures of the $M_J = \pm 3/2$ and $M_J = \pm 1/2$ states. However, if the splittings induced by a [100] and a [111] stress are equal, the off-diagonal terms in the strain-Hamiltonian which give rise to this mixing are zero and M_J is a good quantum number for any orientation of the applied stress. This condition, which is known as *isotropic quantization*, has been shown to hold approximately in silicon [37] and therefore it will be assumed that a similar

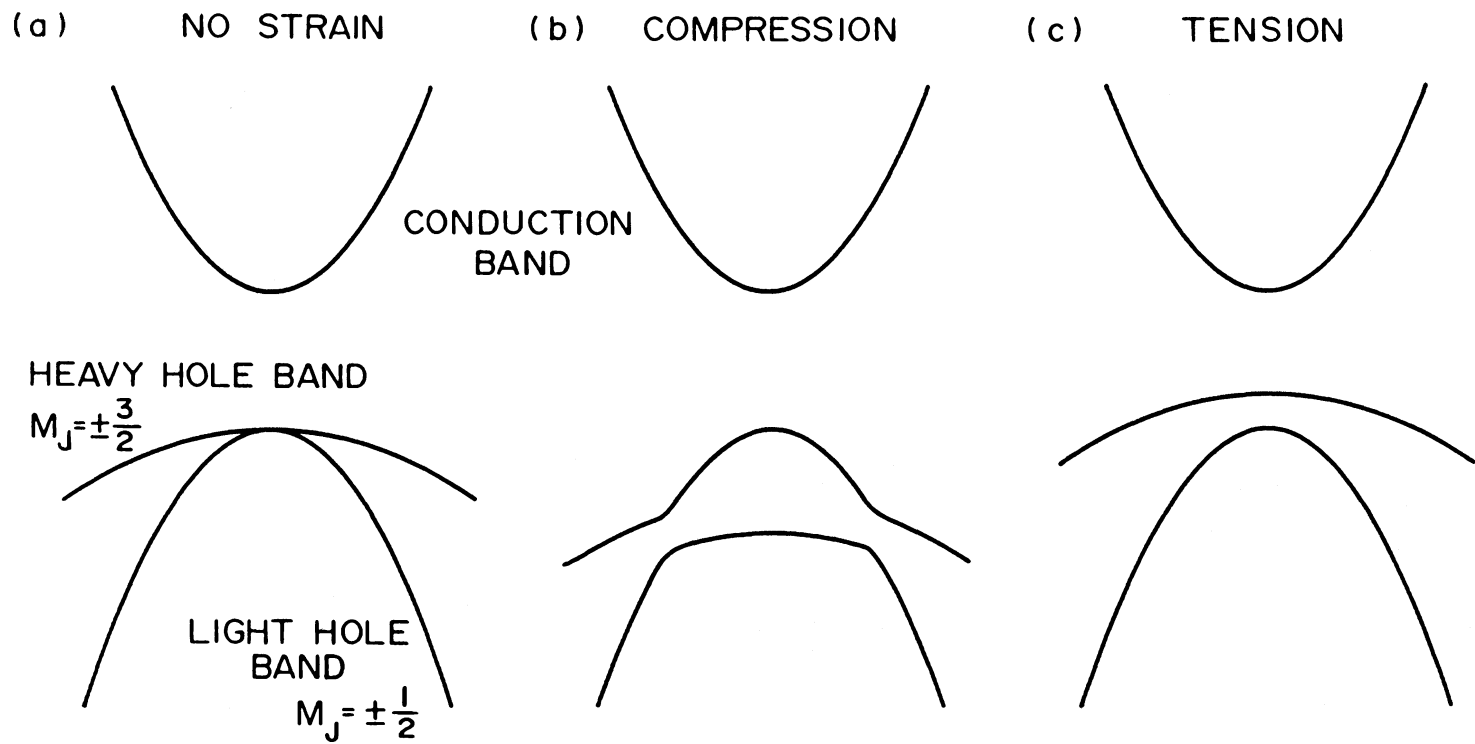


Figure 3.3: Strain-dependence of energy band structure of InGaAsP, with (a) no strain, (b) compression and (c) tension.

relationship applies to InGaAsP. In this case, the quantization axes can be chosen parallel to the [110] crystal axis, *i.e.*, parallel to the stress direction, and the energy band shifts due to an applied stress are the same as in equations (3.28) and (3.29). This assumption is consistent with the experimental results.

The orientation of the quantization axis determines the polarization state of photons emitted in each conduction to valence band transition. Following the notation of Kane [35], the wavefunctions for the conduction, heavy-hole, light-hole and split-off bands are respectively

$$\Psi_c = S \quad (3.30)$$

$$\Psi_{hh} = \frac{1}{\sqrt{2}} (X+iY) \quad (3.31)$$

$$\Psi_{lh} = \frac{1}{\sqrt{6}} [2Z - (X+iY)] \quad (3.32)$$

$$\Psi_{so} = \frac{-1}{\sqrt{3}} [Z + (X+iY)] \quad (3.33)$$

where X , Y , Z are the basis functions which contain the symmetry of the p_x , p_y and p_z atomic orbitals, z defines the quantization axis and S represents an *s-like* wavefunction. The electron spin has been neglected from these equations because a lattice deformation does not affect the spin degeneracy. The intensity of optical transitions is proportional to the matrix element

$$|\langle \Psi_1 | \underline{\epsilon} \cdot \underline{p} | \Psi_2 \rangle|^2 \quad (3.34)$$

where Ψ_1 and Ψ_2 are the final and initial states, \underline{p} is the electron momentum, and $\underline{\epsilon}$ is the polarization vector of the electric field. By symmetry, the only non-zero matrix

elements for conduction band to valence band transitions are

$$M = \langle X | p_x | S \rangle = \langle Y | p_y | S \rangle = \langle Z | p_z | S \rangle . \quad (3.35)$$

Using equations (3.30) to (3.35), one obtains the transition probabilities for the emission of spontaneous photons polarized parallel (I^{\parallel}) and perpendicular (I^{\perp}) to the quantization axis:

For conduction to heavy-hole band transitions

$$I_{c \rightarrow hh}^{\parallel} = 0 \quad (3.36)$$

$$I_{c \rightarrow hh}^{\perp} = \frac{1}{2} M^2 . \quad (3.37)$$

Similarly, for conduction to light-hole band transitions

$$I_{c \rightarrow lh}^{\parallel} = \frac{2}{3} M^2 \quad (3.38)$$

$$I_{c \rightarrow lh}^{\perp} = \frac{1}{6} M^2 \quad (3.39)$$

and for conduction to split-off band transitions

$$I_{c \rightarrow so}^{\parallel} = \frac{1}{3} M^2 \quad (3.40)$$

$$I_{c \rightarrow so}^{\perp} = \frac{1}{3} M^2 . \quad (3.41)$$

In a heavy-hole state, the electron is confined to the plane perpendicular to the quantization axis, *i.e.*, to the stress direction. Hence, the dipole moment for

the emission of light polarized parallel to the stress direction is zero. In the light-hole band, the electron orbit is centred around the quantization axis. Thus, for conduction to light-hole band transitions both polarizations are allowed, but the component parallel to the stress direction is four times stronger. In this experiment the stress direction is parallel to the junction plane. It follows that only TM polarized light is emitted in conduction to heavy-hole band transitions whereas photons emitted in conduction to light hole band transitions are predominantly TE polarized.

The remaining off-diagonal terms in the strain-Hamiltonian introduce a mixing between light-hole and split-off band states [23]. The mixing occurs only between states with $M_J = \pm 1/2$, because M_J is still a good quantum number. The mixing can be expressed as a perturbation to the light-hole band wavefunction

$$\Psi_{lh} = \Psi_{lh} + \frac{\alpha}{\sqrt{2}} \Psi_{so} \quad (3.42)$$

where $\alpha = b\sigma_x/\Delta$, b is a constant which depends on the deformation potential and the elastic properties of the material, Δ is the spin-orbit splitting, and σ_x is the applied stress. Substituting for the perturbed wavefunction in equation (3.34) and using equations (3.30) to (3.35) the transition probabilities become

$$I_{c \rightarrow lh}^{\parallel} = \frac{2}{3} (1 + \alpha) M^2 \quad (3.43)$$

$$I_{c \rightarrow lh}^{\perp} = \frac{1}{6} (1 - 2\alpha) M^2. \quad (3.44)$$

where terms in α^2 have been neglected because for the stresses applied in this

experiment $b\sigma_x \ll \Delta$.

The total transition probabilities for photons polarized parallel (I^{\parallel}) and perpendicular (I^{\perp}) to the stress direction is given by the sum of equations (3.36) and (3.43) and (3.37) and (3.44)

$$I^{\parallel} = \frac{2}{3}(1 + \alpha)M^2 \quad (3.45)$$

$$I^{\perp} = \frac{2}{3}\left(1 - \frac{\alpha}{2}\right)M^2. \quad (3.46)$$

Thus, for a compressive stress ($\alpha > 0$) the mixing of the $M_J = \pm 1/2$ states causes an increase in the transition rate for light polarized parallel to the stress direction and a decrease in the transition rate for light polarized perpendicular to the stress direction.

In a laser with stress applied parallel to the junction plane, this effect corresponds to an increase in the gain of the TE mode and a decrease in the gain of the TM mode. The gain of the TE and TM modes may be written as

$$g_{\text{TE}} = g_o(1 + \alpha) \quad (3.47)$$

$$g_{\text{TM}} = g_o\left(1 - \frac{\alpha}{2}\right) \quad (3.48)$$

where g_o is the gain in the unstressed crystal. These expressions for the strain dependence of the TE and TM mode gains agree with the results of Patel et al. [2] In their work band to impurity level rather than band to band transitions were considered.

Using the values given in [24] and [36] $\alpha \sim -0.02\sigma_x$, where σ_x is the applied stress ($\times 10^9$ dyne/cm²). This value of α corresponds to $\sim 2\%$ change in TE mode threshold and $\sim 1\%$ change in the TM mode threshold for an applied stress of 10^9 dyne/cm². The TE gain decreases and the TM gain increases for a tensile strain. The opposite is true for compression.

3.3 Summary.

In this chapter an expression for the stress distribution which is produced by the probe and two point mounting system has been derived. It was shown that the induced bending moment results in tension or compression in the active region when the laser is positioned with the active up or the active region down respectively. The stress does not vary significantly across the active region and therefore a constant value can be used.

In *Section 3.2* the effect of strain on the valence band structure of III–V semiconductors was discussed. A derivation of the strain dependence of the TE and TM mode gains was presented. It was found that a compressive stress increases the gain of the mode polarised parallel to the stress direction.

In *Chapters 4 and 5* the experimental results will be discussed. It is shown that the measurements of the strain dependence of threshold, wavelength and the polarisation of the output are consistent with the stress distribution and the strain dependence of the valence band wavefunctions presented in this chapter.

CHAPTER 4.
DISCUSSION OF RESULTS.

4.1 Stress dependence of threshold.

The threshold change due to compressive (active layer up, $\sigma_x < 0$) and tension (active layer down, $\sigma_x > 0$) is shown in Fig. 4.1. In these measurements the maximum applied force is close to the breaking point of the laser. Consequently, the probe creates a weakness at the contact point and the laser cleaves at a lower applied stress when it is flipped and deformed in the opposite direction. For this reason the active layer up and active layer down measurements were made on two groups of ten lasers and the average threshold change was plotted. It is apparent that threshold varies linearly with stress and with approximately the same slope for both compression and tension, as expected from equation (3.47). The symmetry of the stress distribution calculated in *Section 3.1* is supported by this result. Experimentally it is found that for an applied stress of 10^9 dyne/cm² the threshold change is $\sim 3\%$. This value is larger than was predicted by the theory presented in *Section 3.2*. This discrepancy maybe due to an inaccuracy in the stress calculation such as neglecting the vertical stress component, or due to the influence of other factors on the gain, such as the strain dependence of the valence band effective mass [19].

Not all the lasers investigated show a simple linear increase in threshold for tensions up to 4×10^9 dyne/cm². Normally, (*i.e.*, without stress) semiconductor diode lasers operate in the TE mode because the reflectivity of the TM mode is lower

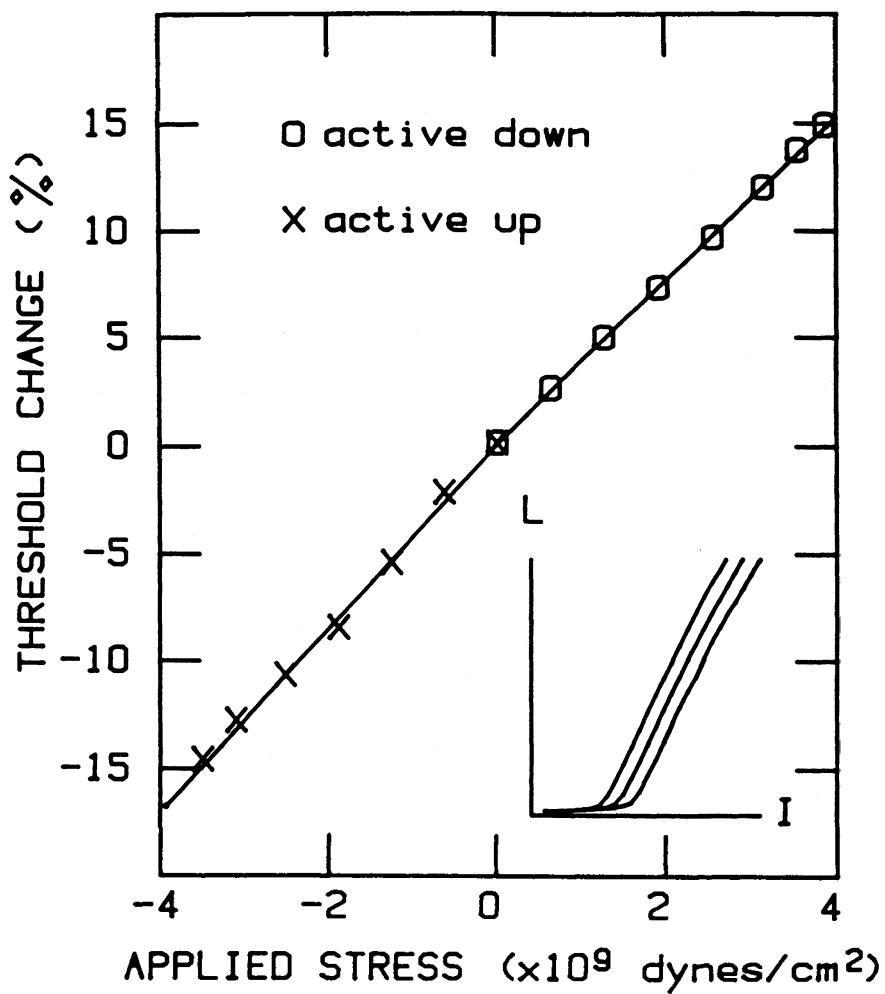


Figure 4.1:

Average relative change in threshold current as a function of the applied stress. Inset, a typical set of *LI*-curves used to determine the stress dependence of threshold.

[38]. As shown in equations (3.47) and (3.48), for a tensile stress the TE gain decreases and the TM gain increases. At a critical stress the increase in the TM gain is sufficient to offset its lower reflectivity and lasing switches to the TM mode. The threshold current increases with stress while the laser is operating in the TE mode and then begins to decrease as the stress is increased beyond the critical value at which a transition to the TM mode occurs. This behaviour, observed with two stripe geometry lasers from the same wafer, is shown in Fig. 4.2(a). It can be seen that for a given applied stress change the rate of increase in the TE mode threshold is larger than the rate of decrease in the TM mode threshold. However, the ratio of the stress dependence of the TE and TM mode thresholds is less than predicted by equations (3.47) and (3.48). This maybe caused by the distortion of the bands at high strains [19].

Previously, the effect of stress on the valence band effective mass [19], or on the rate of intervalence band absorption [20], has been proposed to explain the stress dependence of threshold. However, these theories fail to account for the decrease in threshold above the critical stress. For this reason, it is thought that the effect of strain on the valence band wavefunction is the dominant mechanism in determining the behaviour of diode lasers under stress.

It is interesting that the critical stress corresponding to the transition to TM stimulated emission occurs at approximately the same value for lasers from the same wafer (Fig. 4.2(a)). However, there is a large variation in the critical stress between lasers from different wafers and structures. The threshold current of the PBH laser shown in Fig. 4.2(b) continues to increase for stresses up to 4×10^9 dyne/cm². Thus, the critical stress in this device is much larger compared to

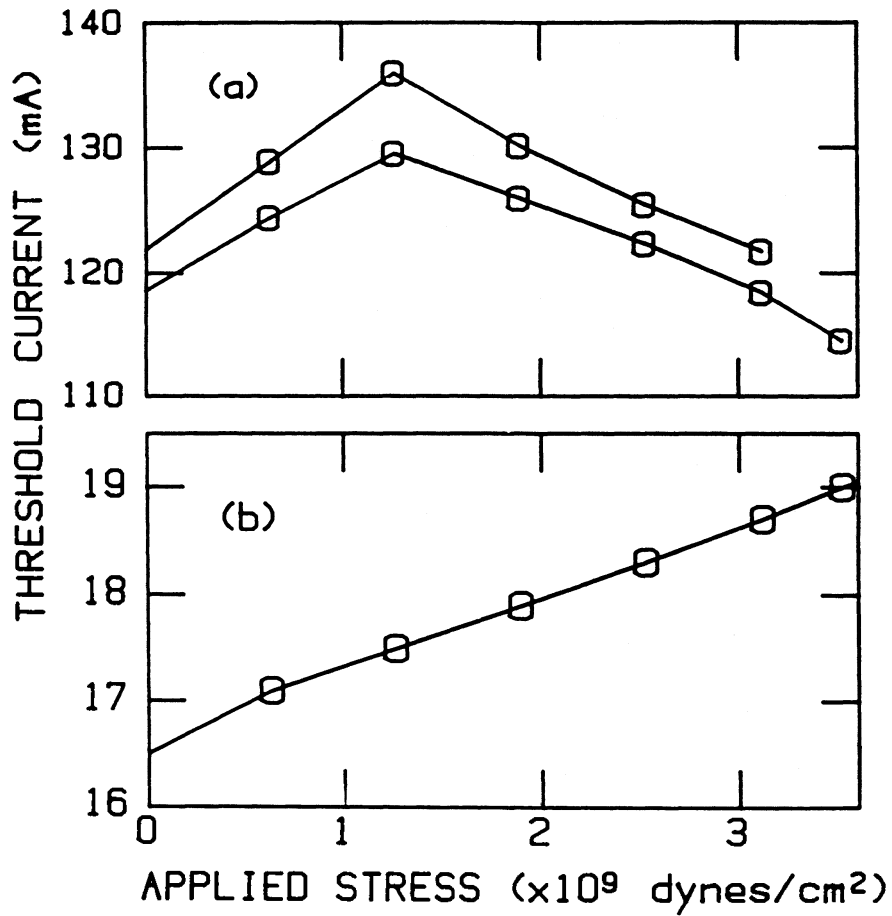


Figure 4.2:

Stress dependence of threshold current for: (a) two stripe geometry DH lasers from the same wafer; and, (b) a PBH laser.

stripe geometry DH lasers. There are a number of possible explanations for this difference: If the distance between the centre plane and the active region varies between wafers then the stress within the active region will not be given accurately by equation (3.26). This could account for the observed variation of the critical applied stress. However, for all lasers used in this study, the position of the active region, relative to the centre plane, is approximately constant. A second possible explanation is that there is a larger difference between the TE and TM mode reflectivities in the PBH structure. But the symmetry of the far-field in the vertical and horizontal directions, for this structure, means that the TE and TM mode reflectivities should be approximately equal [38]. Therefore, the reason that these PBH lasers did not show a transition to TM emission is thought to be that there exists a large fabrication stress in the active region, which acts to favour the TE mode. The effects of fabrication stresses are considered in more detail in relation to the polarisation of the spontaneous emission in *Section 5.1*.

4.2 Stress dependence of the wavelength.

Further support for the strain-dependent valence-band wavefunction picture is provided by measurements of the emission wavelength with the active region under tension and compression. The lasers operate multimode with $\sim 4-6$ longitudinal modes lasing simultaneously. The wavelength of each individual mode depends on the refractive index of the active layer which changes as stress is applied. The wavelength shifts of the individual modes does not tell us about the energy band shifts and therefore it is more useful to study the wavelength of the gain peak

maximum. This was measured using a 1/2-meter monochromator, with the entrance and exit slits opened up such that the resolution was between one and two mode spacings. The wavelength setting on the monochromator was adjusted until the maximum output signal was obtained. This wavelength corresponds to the gain peak wavelength.

The wavelength of the gain peak maximum for a stripe geometry DH laser as a function of the applied stress is shown in Fig. 4.3. At zero stress the stimulated emission is TE polarized. For positive stress (tension) the wavelength increases, *i.e.*, the bandgap decreases. For negative stress (compression) the wavelength decreases, *i.e.*, the bandgap increases. These results agree with the energy band shifts described in equations (3.28) and (3.29). The variation of the TE gain peak wavelength corresponds to an energy shift of $0.6 \text{ meV}/(10^9 \text{ dyne/cm}^2)$. At a critical tension of $1.3 \times 10^9 \text{ dyne/cm}^2$ there is a jump in wavelength and the polarization changes to TM. This point corresponds to the critical stress at which there is a transition from threshold increasing to threshold decreasing as shown in Fig. 4.2(a). Conduction to heavy-hole type transitions emit TM light whereas conduction to light-hole transitions emit predominantly TE light. Therefore, in Fig. 4.3 the wavelength difference between TE and TM polarised light at the critical stress corresponds to the splitting between the light- and heavy-hole band shown in Fig. 3.3(c). Above the critical stress the lasing wavelength continues to increase but with a steeper gradient, corresponding to an energy shift of $3 \text{ meV}/(10^9 \text{ dyne/cm}^2)$. This is due to the larger energy shift with stress of the heavy-hole band given in equation (3.28) and (3.29). Although the ratio of the light- and heavy-hole band shifts agrees with previous work [25,26] the magnitude of the wavelength changes are only one-half that

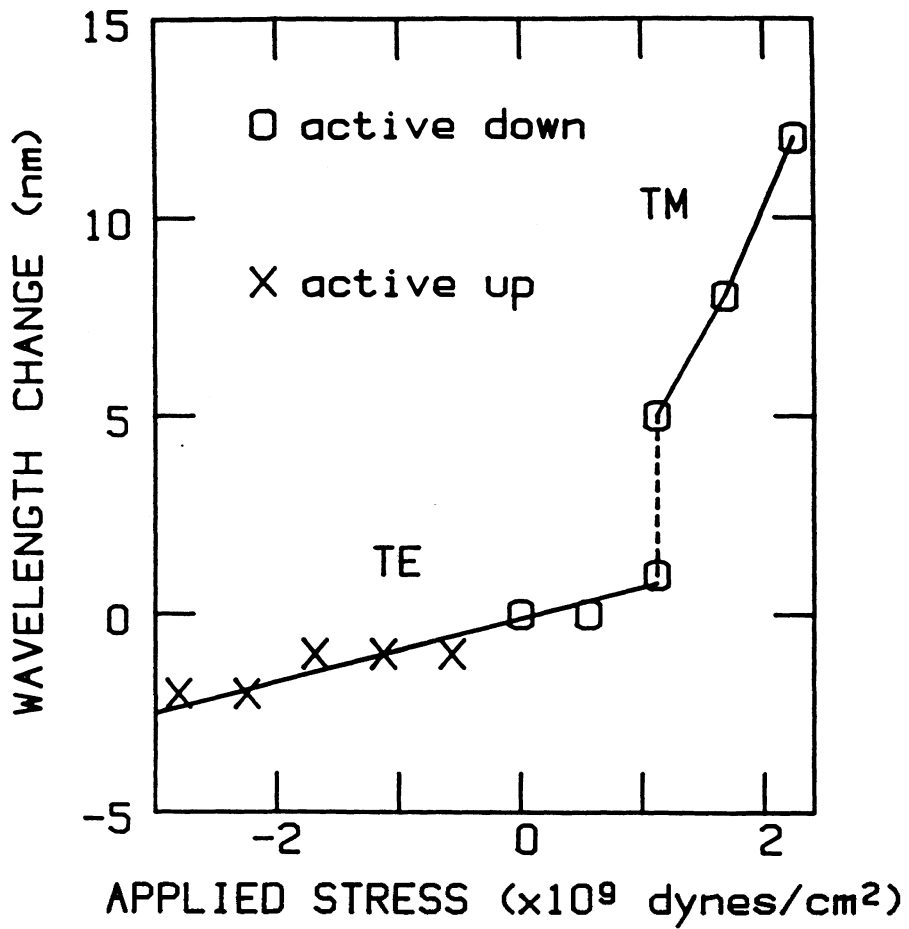


Figure 4.3:

The wavelength corresponding to the maximum gain as a function of the applied stress was measured on a sample of lasers. Shown here are the results typical of stripe geometry DH lasers.

predicted by equations (3.28) and (3.29). This implies that the selection rules presented in *Section 3.2* are not obeyed rigorously but that both polarisation states are allowed for light- and heavy-hole transitions. Alternatively, if the strain changes the curvature of the bands [18] the quasi-Fermi level shifts will not be the same as the band-edge shifts and therefore the variation of the wavelength of emission is not given accurately by equations (3.28) and (3.29).

4.3 Effects of contact stress.

For the results reported in *Section 4.1* and *4.2* the experiments were performed such that the contact or Hertzian stresses could be neglected by placing the probe off to one side of the stripe, *i.e.*, 20 μm away from the active region. By doing so, it has been possible to compare the effects of tension and compression on the performance of a single laser chip simply by flipping it over. However, the dependence of threshold and wavelength on the Hertzian stresses provides further support to the theory of optical transitions in strained semiconductors presented in *Chapter 3*. Therefore this section is devoted to a discussion of the effect of the Hertzian stresses on the properties of semiconductor diode lasers.

The experiments on contact stress were performed by placing the probe directly above the stripe, *i.e.*, the lasers were placed with their active region up. The application of a force close ($\sim 2 \mu\text{m}$) to the active region often led to damage of the laser and so these experiments could only be performed on lasers which were not needed for further analysis. A comparison between the effect of the bending stress

and the Hertzian stresses on the threshold of five lasers was made. The LI -curves for three values of the applied force with the probe positioned $\sim 20 \mu\text{m}$ away from the stripe and then directly above the stripe are shown in Fig. 4.4(a) and Fig. 4.4(b) respectively. For a compressive stress parallel to the junction plane (bending stress) the threshold current decreased with increasing applied force as shown in Fig. 4.4(a). However, with the probe directly above the active region (contact stress) threshold increased with applied force as shown in Fig. 4.4(b). The rate of change of threshold with applied force due to the contact stress is roughly a factor of five larger than that due to the bending stress. This suggests that the magnitude of the Hertzian stress for a particular applied force is larger than the corresponding bending stress.

As the direction of the threshold change due to the Hertzian stress is opposite to the effect of bending the direction of the dominant Hertzian stress component can be predicted. It is known that the effect of an applied compressive stress is to decrease the gain of the mode polarised perpendicular to the stress axis. Therefore, since the TE mode threshold increases, the contact must produce a net compression which is perpendicular to the junction plane. If the gain of the TE mode decreases then the gain of the TM mode must increase. Hence, it is expected that the application of Hertzian stress will produce lasing in the TM mode. This expectation was confirmed experimentally. However, the effect of contact stress on the polarization of the output is different than the effect of bending induced stress. When stress was applied to lasers with their active region down (*i.e.*, bending stress) there occurred an abrupt transition from TE to TM polarized stimulated emission. However, the effect of the contact stress is to gradually rotate the plane of polarization from parallel (TE mode) to perpendicular (TM mode) to the junction

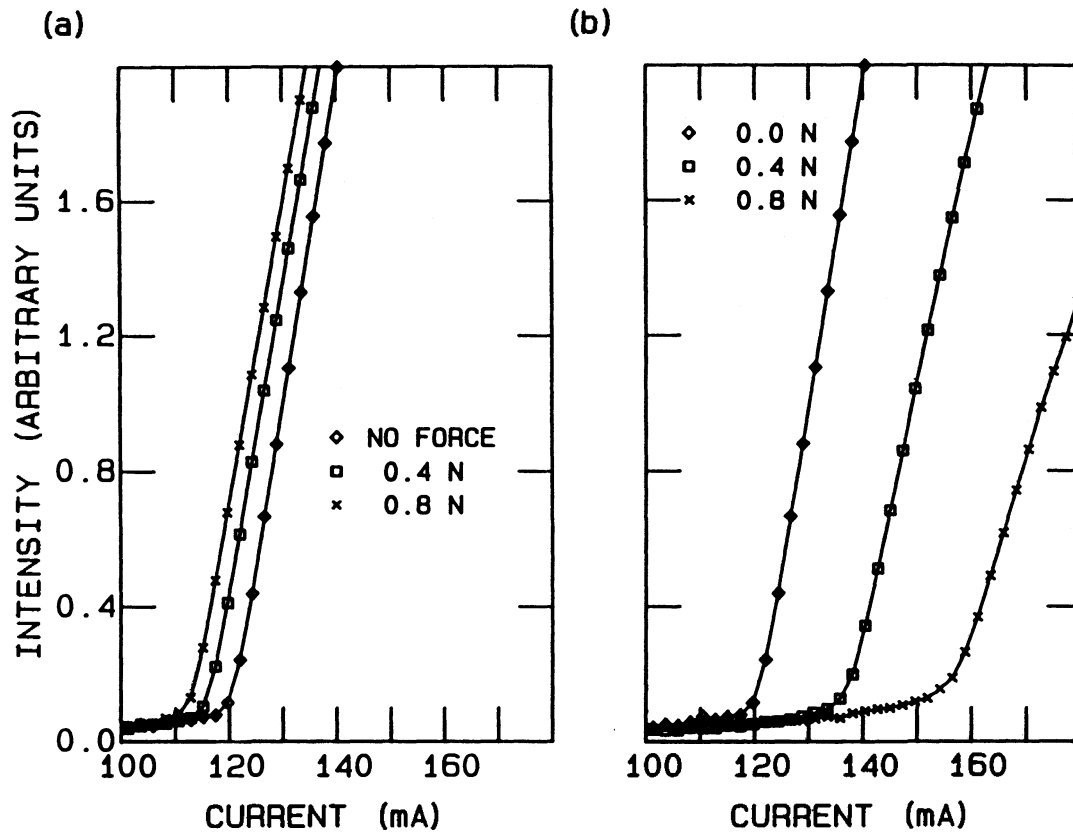


Figure 4.4:

Comparison of the effect of contact and bending stress on threshold. The LI -curve of a stripe geometry DH laser for three values of the applied force with the probe placed (a) $20 \mu\text{m}$ to one side (bending) and (b) directly above the stripe (contact).

plane. This implies that there is a complex deformation of the lattice within the active region and therefore, the theory presented in *Chapter 3* is inappropriate.

A second effect of the Hertzian stresses, which is not observed under bending, is that the efficiency of the laser is reduced, see Fig. 4.4(b). This implies that as well as changing the gain of the lasing mode, the stress also has an effect on the loss. It has been suggested that hydrostatic pressure increases the rate of intervalence band absorption [20]. This effect would explain the observed decrease in efficiency with increasing stress and possibly account for the large threshold change. However, the results of an investigation of the dependence of the emission wavelength on the Hertzian stress are inconsistent with the intervalence band absorption assumption.

The wavelength of emission as a function of the applied force with the probe directly above the stripe was measured. It was found that the wavelength decreases with increasing applied force. This corresponds to an increase in the bandgap as expected from the strain-dependence of the energy bands (see Fig. 3.3). The rate of decrease of the emission wavelength with respect to the applied force with the probe directly above the active region is greater by a factor of five than with the probe off to one side. This difference is the same as for the rate of change of threshold with applied force and therefore it is thought that the magnitude of the Hertzian strain is five times larger than the bending stress for the same applied force.

Another effect of the Hertzian stress distribution is to change the shape of the LI -curve of stripe geometry DH lasers at high optical output powers. The behaviour of index-guided (buried heterostructure) and gain-guided (stripe geometry double heterostructure) lasers at high optical power levels is different. For an

index-guided laser the relationship between output power and current is approximately linear up to the peak power. In this case, the peak power is limited by catastrophic optical damage to the mirror facets or thermal runaway [39]. For a gain-guided lasers the output power begins to roll-off at high currents and it is this roll-off which limits the maximum output power of the device. The peak output power and the current at which the roll-off begins varies from laser to laser. The laser driver used, in these experiments, provided a maximum current of $\sim 230\text{mA}$. Therefore only lasers which have a roll-off at a current less than this value were studied. This roll-off combined with relatively high threshold (generally $\sim 100\text{ mA}$) means that the performance of these lasers is very poor compared to more recent technology. However, their behaviour when subjected to an applied stress is interesting and provides insights into the physics of lasing.

If the lasers are positioned with the active region down then the effect of the applied stress is to increase threshold but does not produce a significant change in peak output power. If the lasers are positioned with the active region up and the probe is placed within $10\ \mu\text{m}$ of the stripe, the applied force has a dramatic effect on the maximum output. The effect of the applied stress on the roll-off of a stripe geometry DH laser is shown in Fig. 4.5. With no applied stress the output power saturates at $\sim 4\text{ mW}$. As stress is applied there is a jump in the output power at a particular current. This jump occurs at a progressively lower current as the stress is increased. If sufficient stress is applied the kink disappears and the LI -curve looks similar to its original form, except that now the maximum optical power is greater than $\sim 7\text{ mW}$. The observation of this effect depends critically on the position of the probe. This means that the phenomenon must result from the Hertzian stress

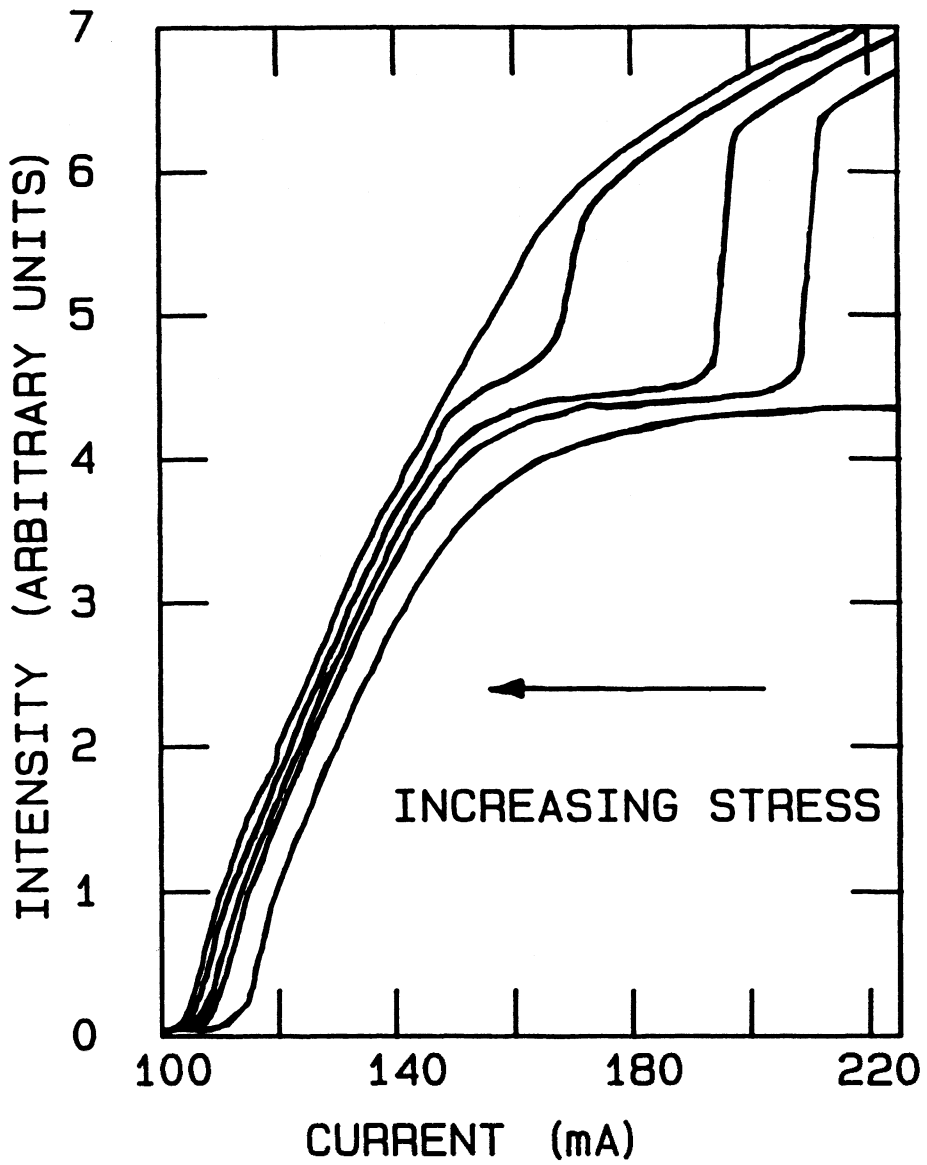


Figure 4.5: A series of *LI*-curves of a stripe geometry DH laser with increasing applied force. The probe is positioned close to the active region. As the force is increased a higher peak output power is obtained.

distribution. The exact form of the contact stress is unknown therefore it is impossible to make anything more than speculative statements on this subject. However, we do know that the contact produces a large stress variation of the order of 10^9 dyne/cm² within a distance of $\sim 10\text{--}20$ μm (see discussion in *Chapter 2*). This stress gradient is perhaps sufficient to give photoelastic guiding of the lasing mode [15]. This provides a possible explanation for the roll-off. The roll-off could occur due to a breakdown of gain-guiding at high output power. (This would explain why similar behaviour is not observed in index-guided lasers because in this case the guiding mechanism is built-in). By producing a stress distribution within the active region of a gain-guided laser it is possible to induce some index guiding by the photo-elastic effect. This index-guiding shifts roll-off to a higher output power, *i.e.*, the behaviour becomes more like that of an index-guided laser.

4.4 Far-field pattern.

It is known that stress within the active region of a diode laser produces a refractive index change which can result in waveguiding of the lasing mode [15]. Also the observation of kinks in the *LI*-curve of buried heterostructure lasers has been demonstrated to be associated with the threshold of higher order TM modes [16] due to stress within the active region. The possible appearance of higher order spatial modes and photoelastic waveguiding due to an applied stress was investigated by measuring the far-field pattern of the lasers.

The far-field pattern was determined by translating the detector across the beam, with a separation of a few centimeters between the laser and the detector.

The detector is moved using a stepper motor (Compumotor CX 5751) and a micropositioner. An angular resolution of $\sim 1^\circ$ can be achieved with this technique. The amount of light which falls on the detector is relatively small and it is necessary to use an amplifier (HP 461A) to increase the output signal. A typical far-field pattern consists of fifty points between $\pm 40^\circ$. Each point is the average of fifty readings, to reduce the amplifier noise.

The far-field patterns of a stripe geometry DH laser with no applied stress and under an applied tension $\sigma_x \sim 3.4 \times 10^9$ dyne/cm² are shown in Fig. 4.6. The intensity is reduced when a tensile stress is applied due to the increase in threshold. However, the angular distribution of the light is not changed by the application of stress. This means that the applied stress does not produce significant photoelastic waveguiding. A similar result was obtained with the buried heterostructure laser. This result is expected from the stress calculation in *Section 3.1*, where we were able to assume a constant value for the stress within the active region. Photoelastic waveguiding requires a stress difference of $\sim 10^9$ dyne/cm² [15] between the active region and the surrounding layer which does not occur with our technique. It is possible, that the Hertzian stresses due to the contact may have the required gradients to induce some guiding. This possibility was discussed in relation to the roll-off of the *LI*-curve of gain-guided lasers in *Section 4.3*.

The far-field patterns shown in Fig. 4.6 were measured with the laser operating in the TE mode. It is more interesting, to compare the angular distribution of TE and TM polarized light. These experiments were performed on diodes which lase in the TM mode or a mixture of TE and TM modes when a tensile stress is produced in the active region. For a laser which has completely TE polarized

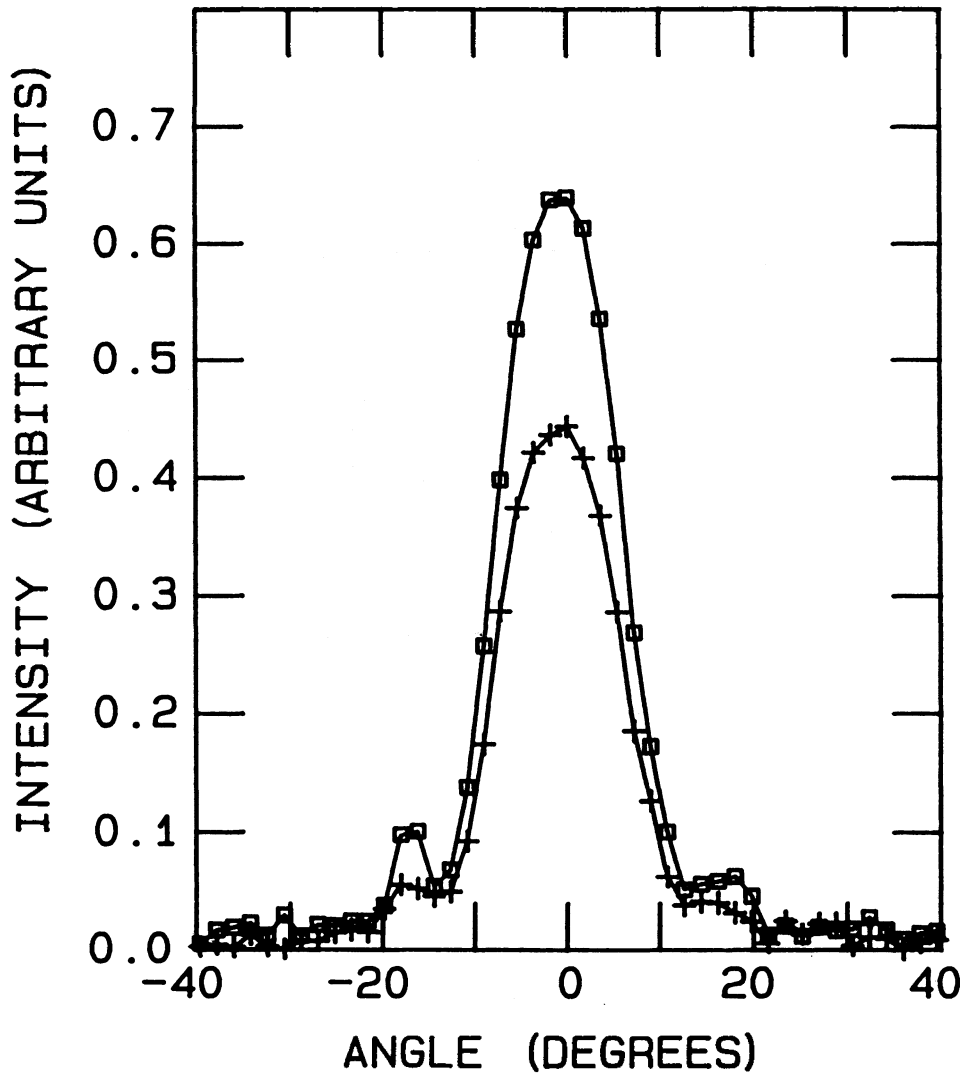


Figure 4.6:

Far-field pattern of a stripe geometry DH laser with no applied stress and $\sigma_x \sim 3 \times 10^9$ dyne/cm². The applied stress affects the amplitude but not the angular distribution of the output.

stimulated emission with no applied stress, and almost completely TM stimulated emission above a critical applied stress, the TE and TM mode far-field pattern can be measured without the use of a polarizer. In this case, the device is lasing independently in one or the other polarization mode and it is found, that the far-fields are very similar.

Finally, the polarization resolved far-field patterns were measured with the device lasing simultaneously in the TM and TE modes. About 30% of the buried heterostructure lasers in this study lase in a mixture of the TE and TM modes when the applied stress is increased beyond the threshold value for the appearance of TM stimulated emission. (The polarization behaviour of those devices is discussed in *Section 5.1*). These lasers have non-ideal far-field patterns with many peaks and troughs. The lasers were positioned with the active region down and a force was applied until simultaneous lasing of the TE and TM modes was observed. The angular distribution of the TE and TM polarized light was measured using a polarizing filter designed for use at $1.3 \mu\text{m}$ (Oriel 27360). The results are shown in Fig. 4.7. Although the far-field patterns of the TE and TM modes are different, the peaks in both distributions tend to occur at the same angles. This means that the TE and TM modes oscillate in similar spatial modes. The overlapping of polarization spatial modes was also observed with stripe geometry DH lasers. These lasers display an abrupt transition from TE to TM polarized stimulated emission as the applied stress is increased. However, at a critical applied stress they appear to lase simultaneously in both polarization modes. The polarization resolved far-field of a couple of stripe geometry DH lasers was measured at this critical stress. It was found that the TE and TM modes had the same angular distribution.

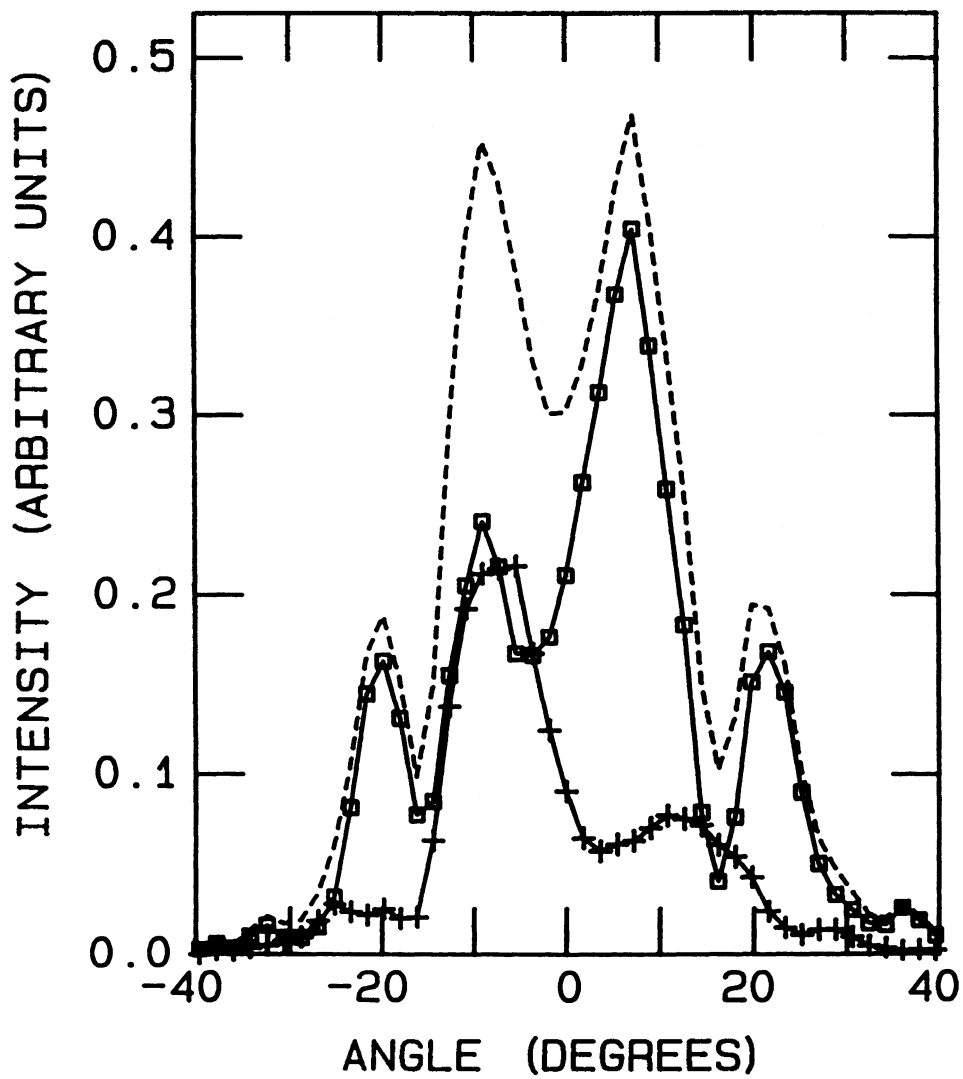


Figure 4.7:

Polarization resolved far-field pattern of a non-ideal PBH laser.

The TE mode intensity (□), TM mode intensity (+) and the

total output power (broken line) are shown.

These results do not support the work of Dutta *et al.* [16] which suggested that the TE and TM mode do not overlap in space. He observed that lasing in the TM mode occurs in a higher order spatial mode and therefore, is supplied by parts of the population inversion which are not used by the TE mode.

4.5 Summary.

In *Section 4.1* it was shown that the threshold variations due to an externally applied stress are consistent with the theory presented in *Chapter 3*. With the active region under tension some lasers show a transition to TM polarised stimulated emission at a critical applied stress. The value of the critical applied stress varied between lasers but was approximately constant for lasers from the same wafer. It was suggested that the value of the critical applied stress is related to the internal stress in the active layer.

The results of measurements of the wavelength of emission as a function of the applied stress were shown to be consistent with the strain dependent energy band shifts discussed in *Section 3.2*.

In *Section 4.3* a comparison between the effects of bending stress and contact stress on the performance of the lasers was made. It was found that contact stress produced effects which are not observed with bending stress such as a rotation of the plane of polarisation of the stimulated emission and an increase in the saturation output power of stripe geometry DH lasers.

Finally, the effect of stress on the far-field pattern of the laser output was investigated. The applied stress was observed to have no effect on the angular

distribution of the laser emission. In measurements of the polarisation resolved far-field pattern it was shown that when both polarisation modes lase simultaneously they appear to occupy the same spatial mode.

At a critical applied stress the laser appears to operate in the TE and TM modes simultaneously. In *Sections* 5.1 and 5.2 the lasers are biased with the critical applied stress and the effect of current and temperature on the polarisation of the output is investigated.

The results of this chapter all concern the above threshold behaviour of semiconductor diode lasers under an externally applied stress. In *Section* 5.3 measurements of the strain dependent behaviour below threshold will be reported and discussed.

CHAPTER 5.
POLARISATION EFFECTS.

5.1 Polarisation resolved LI-curve.

In *Chapter 4* it was found that if the lasers are positioned with the active down and a stress is applied the stimulated emission changes from TE polarised to TM polarised. At a critical applied stress corresponding to this transition both polarisation modes appear to lase simultaneously. If the applied stress is set at the critical value such that the output powers in the TE and TM modes are approximately equal, then the polarization state of the output becomes very sensitive to small changes in the stress distribution within the device. This sensitivity can be used to investigate stresses produced by current-induced heating or changes in the ambient temperature. In *Section 2.2* a discussion of thermal effects and how they can be avoided was presented. In this section, thermal stress will be discussed. The appearance of thermal stress when the lasers are being operated with short current pulses and a low duty-cycle should be clarified. Even within the initial 200 ns of the current pulse, there occurs some heating of the active region. The induced temperature rise causes a thermal stress $\sim 10^6$ dyne/cm². These thermal stresses will be considered in *Sections 5.1* and *5.2*.

The effect of current on the stress distribution were studied by measuring the polarization resolved LI-curve of lasers subjected to the critical applied stress. The applied stress was adjusted to give equal output in the TE and TM modes at a current $\sim 50\%$ above threshold. The polarization resolved LI-curves for a PBH and

stripe geometry DH laser are shown in Fig. 5.1. For the PBH laser (Fig. 5.1(a)) the polarization of the stimulated emission just above threshold is TE. At a current of ~ 45 mA there is a transition to predominantly TM polarized stimulated emission. For the stripe geometry laser shown in Fig. 5.1(b) the output is TM polarized just above threshold and at ~ 170 mA there is a transition to the TE mode.

This switching behaviour can be explained in terms of the current-induced stress. The laser is biased with an applied stress close to the critical stress which results in a transition between polarization modes. A small stress change due to current-heating is sufficient to take the device through the transition, giving lasing in the other mode. It is apparent from Fig. 5.1 that in the PBH laser the current induced stress promotes the TM mode whereas in the stripe geometry DH laser the TE mode is favoured at higher current. This difference may be explained in terms of the structure of each device. In the PBH structure the active region consists of a *strip* of quaternary InGaAsP surrounded by InP. In the stripe geometry DH laser the active region is formed by a plane of InGaAsP between InP cladding layers. The thermal expansion coefficient of the quaternary is larger than for InP. With current injection heat is generated in the active region which tries to expand more than the surrounding crystal and therefore induces a stress. In the PBH device there is stronger current confinement and the heating is more restricted in the lateral direction. This has the result that the vertical component of the current-induced stress is more important. A compressive stress perpendicular to the junction plane increases the gain of the TM mode. Therefore, the TM mode is favoured at higher currents. In the stripe geometry DH structure, with poorer current confinement, and no compositional change in the lateral direction, the horizontal component of the

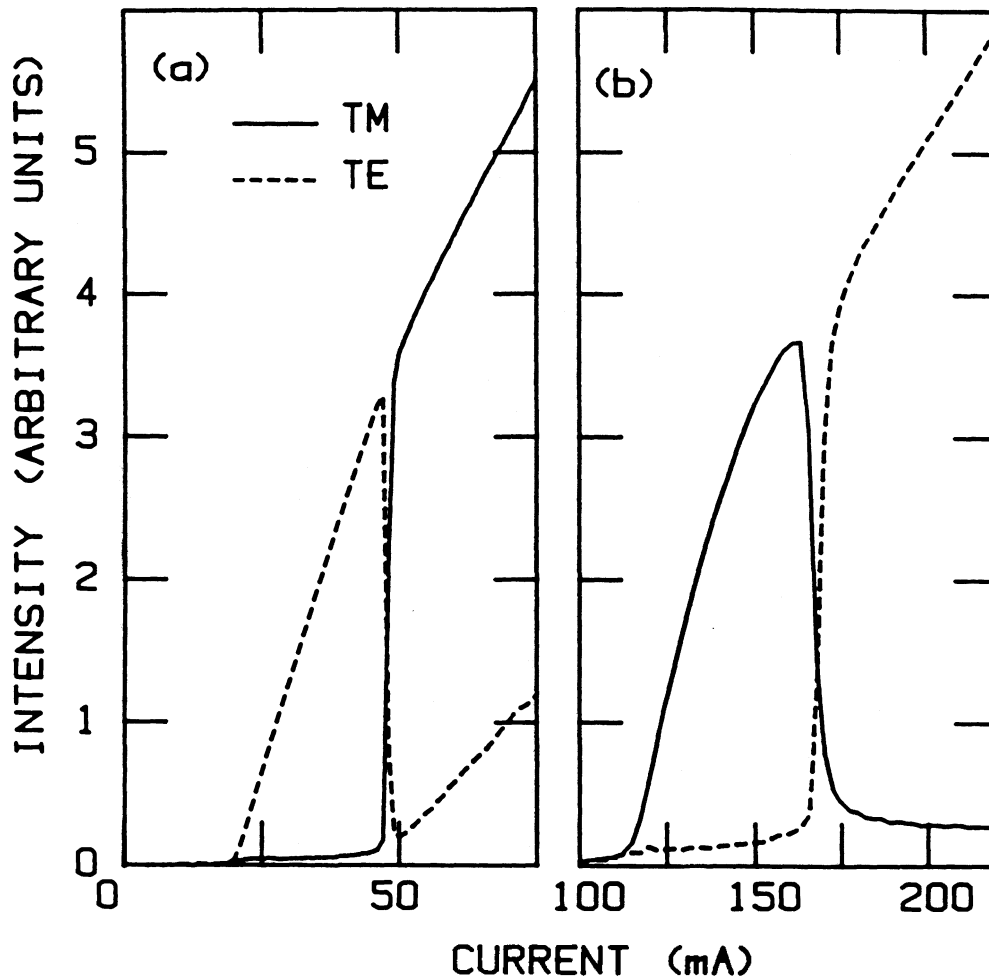


Figure 5.1:

Polarization resolved LI -curves for (a) a PBH and (b) a stripe geometry DH laser biased with the critical applied stress. The transition between polarization modes is caused by the current-induced thermal stress. The different behaviour can be explained by the structure of each device.

thermal stress is more important. Hence, the TE mode is observed at higher injection levels.

About 30% of the PBH lasers studied show very different polarisation behaviour. In these devices, there was no sharp transition from the TE to the TM mode at the critical stress. Instead, above a particular stress, simultaneous lasing in the TE and the TM modes was observed. A further increase in the applied stress increases the relative amount of TM polarised light. However, in contrast to the behaviour of the stripe geometry DH lasers, the TE mode was not extinguished completely above the transition. The polarisation resolved LI -curve of this type of laser is shown in Fig. 5.2(a). Just above threshold only the TM mode is lasing. At higher currents both modes lase simultaneously. This behaviour is very different from the other PBH lasers, discussed earlier in this chapter. An explanation of this effect in terms of a simple thermal stress model is not possible. These lasers have non-ideal far-field patterns (see *Section 4.4*) which may help to explain their strange polarisation behaviour.

The polarisation resolved LI -curve at the critical stress of stripe geometry DH lasers with a different structure was investigated. These lasers have a quaternary first confining layer instead of the conventional InP first confining layer. The polarisation resolved LI -curve of four Q -confining lasers was measured. Each of the lasers in this sample displayed similar behaviour. A typical curve is shown in Fig. 5.2(b). Both polarisation modes lase just above threshold. At higher current the TE mode dies away leaving the TM mode to dominate. This behaviour is opposite to the conventional stripe geometry DH lasers which suggests that changing the composition of one layer has a significant effect on the thermal stress within the

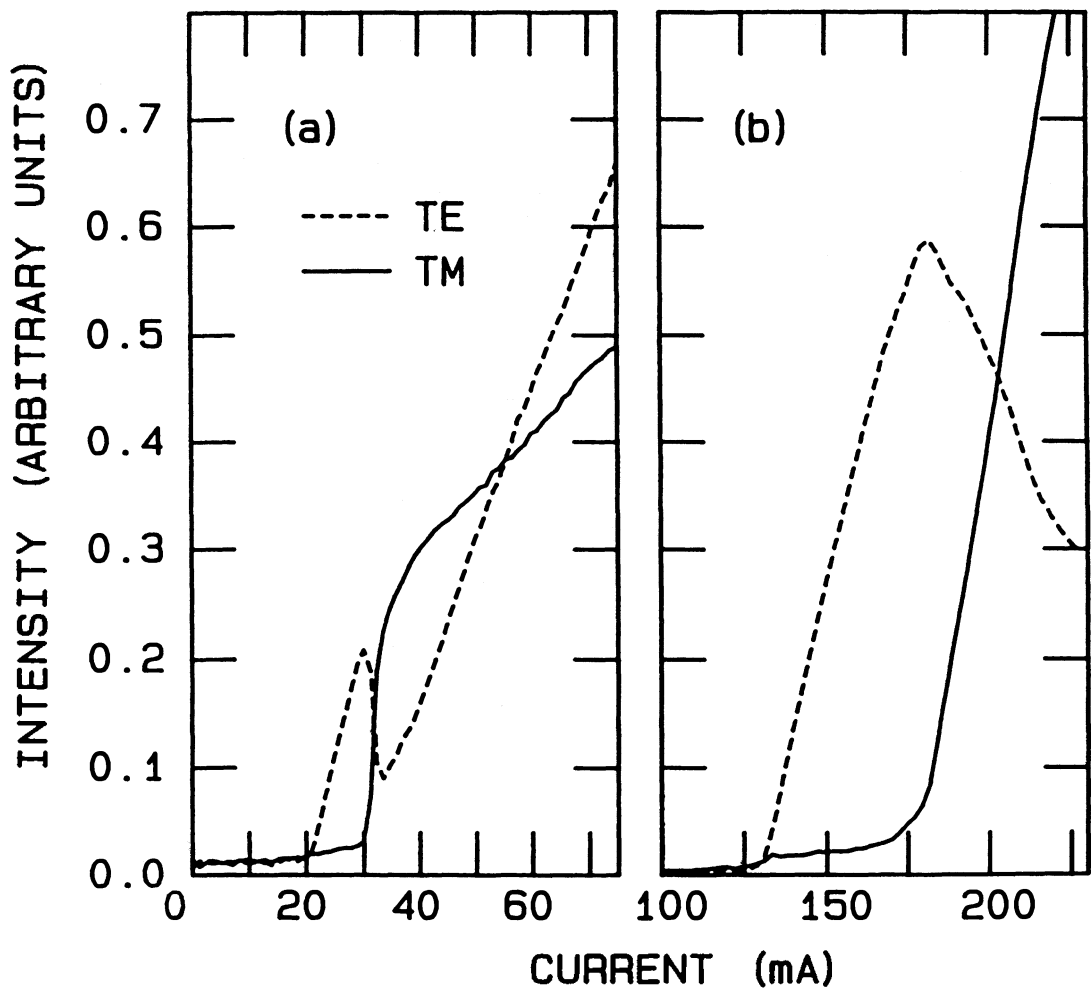


Figure 5.2: Polarization resolved LI -curve for (a) non-ideal PBH laser and (b) a Q-confining stripe geometry DH laser at the critical applied stress.

active region. The effect of composition on thermal stress has been discussed by Chen *et al.* [10]. They suggest that by inserting a quaternary buffer between the active layer and the first confining layer, the thermal stresses caused by cooling the lasers from the LPE growth temperature can be compensated.

Although the polarisation behaviour of different lasers at the critical stress appears varied, it is possible to observe some similarities between different devices by changing the heat-sink and the applied stress simultaneously. A diode which lases in the TM mode just above threshold with a transition to the TE mode at higher current can be made to lase in the TE mode just above threshold and the TM mode at higher current by increasing the heat-sink temperature and increasing the applied stress. To explain the polarisation LI -curve an exact knowledge of the current-induced stress, the thermal stress at a particular heat-sink temperature, and the applied stress is needed. This analysis would require a finite-element approach to the stress calculation, which is outside the range of this work.

A similar transition between polarization modes as the current is increased was observed by Chen and Lui at low temperature [9]. Cooling the lasers creates a thermal stress within the active region which is equivalent to the tensions produced in this experiment. Chen and Liu found that in some lasers this polarization transition was bistable [40]. In this work no bistability is observed. The absence of bistability is believed to be due to the fact that in this work measurements are performed at room temperature and therefore kT is larger than the stress induced splitting between the light- and heavy-hole bands. At low temperatures ($kT \ll$ splitting) and there is an asymmetry between the light- and heavy-hole band populations which depends on which polarization mode is lasing. This dependence

results in a self-stabilization of the lasing mode and therefore bistability.

The transition between polarisation modes could occur by a rotation of the plane of polarisation or by the *inhibition mechanism* which means that one polarisation mode completely replaces the other [41]. A critical stress was applied to a stripe geometry DH laser such that a polarisation transition was observed. Then the polarising beam splitter cube was rotated to transmit the light polarised at 45° to the TE and TM directions and the LI -curve was measured. The 45° curve was equal to half the unpolarised LI -curve which means that the polarisation transition occurs by the inhibition mechanism. If the transition occurred by rotation, a peak or trough in the 45° curve at the transition current would be observed. In this experiment the polarisation transition is induced by an applied stress. A similar result was obtained when the transition was induced by cooling [41].

In about 70% of the stripe geometry DH lasers studied there occurs a repeated switching between polarization modes as the current is increased. The second transition between the TE and TM mode cannot be explained by a current-induced thermal stress. In this case, it is thought that the current-induced stress does not predominantly favour one particular mode and therefore other effects become important. The observed multiple switching shown in Fig. 5.3 maybe the result of a coupled mode condition caused by the non-uniformity of the stress distribution along the laser cavity.

A series of polarisation resolved LI -curves showing the TM mode as the applied stress was increased in increments of $\Delta\sigma_x \sim 5 \times 10^5$ dyne/cm² is shown in Fig. 5.4. At the lowest stress the stimulated emission is mostly TE polarised. As the stress is increased, a characteristic polarisation resolved LI -curve similar to Fig.

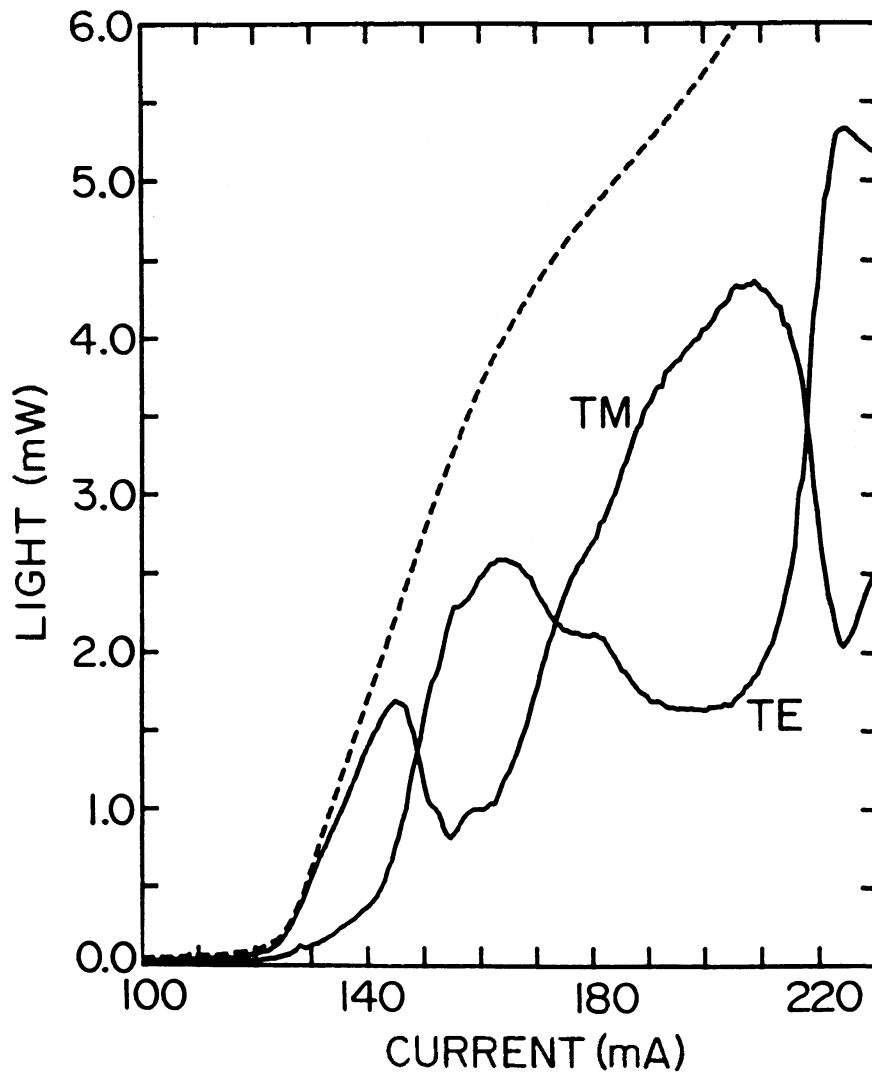


Figure 5.3:

Example of the multiple switching observed at a critical applied stress in $\sim 70\%$ of the stripe geometry DH lasers tested. The total output power is plotted with a broken line.

5.1 – 5.3. is observed. This device lases in the TM mode just above threshold. The TE mode intensity peaks at ~ 180 mA. The TM mode dominates again at higher current. At higher stress the kink in the TM mode intensity shrinks, until at the maximum stress the stimulated emission occurs completely in the TM mode and the LI -curve above threshold is approximately linear.

An alternative method of investigating the current-induced stress is to examine the polarization resolved transient pulse behaviour with the laser biased at the critical applied stress. For the PBH laser the light pulse is initially TE polarized and then switches to the TM mode. The time between the beginning of the pulse and the polarization transition depends upon the current level and the applied stress. However for the stripe geometry DH laser, the pulse turns on in the TM mode and switches to the TE mode at a later time. The behaviour illustrates that the current-induced thermal stress favours TE emission in the stripe DH structure and TM emission in the PBH structure, as discussed above.

5.2 Measurement of thermal stress.

A technique to measure the current-induced stress using the polarization mode transition has been developed. The TM mode LI -curve for a stripe geometry DH laser biased with the critical applied stress is shown in Fig. 5.5(b). The dashed curve corresponds to a measurement made 100 ns after the beginning of the pulse. If the measurement is made $1 \mu\text{s}$ after the beginning of the pulse, then the extra current-induced heating has increased the temperature of the active region resulting in an increase in threshold and a thermal stress change, which shifts the transition to

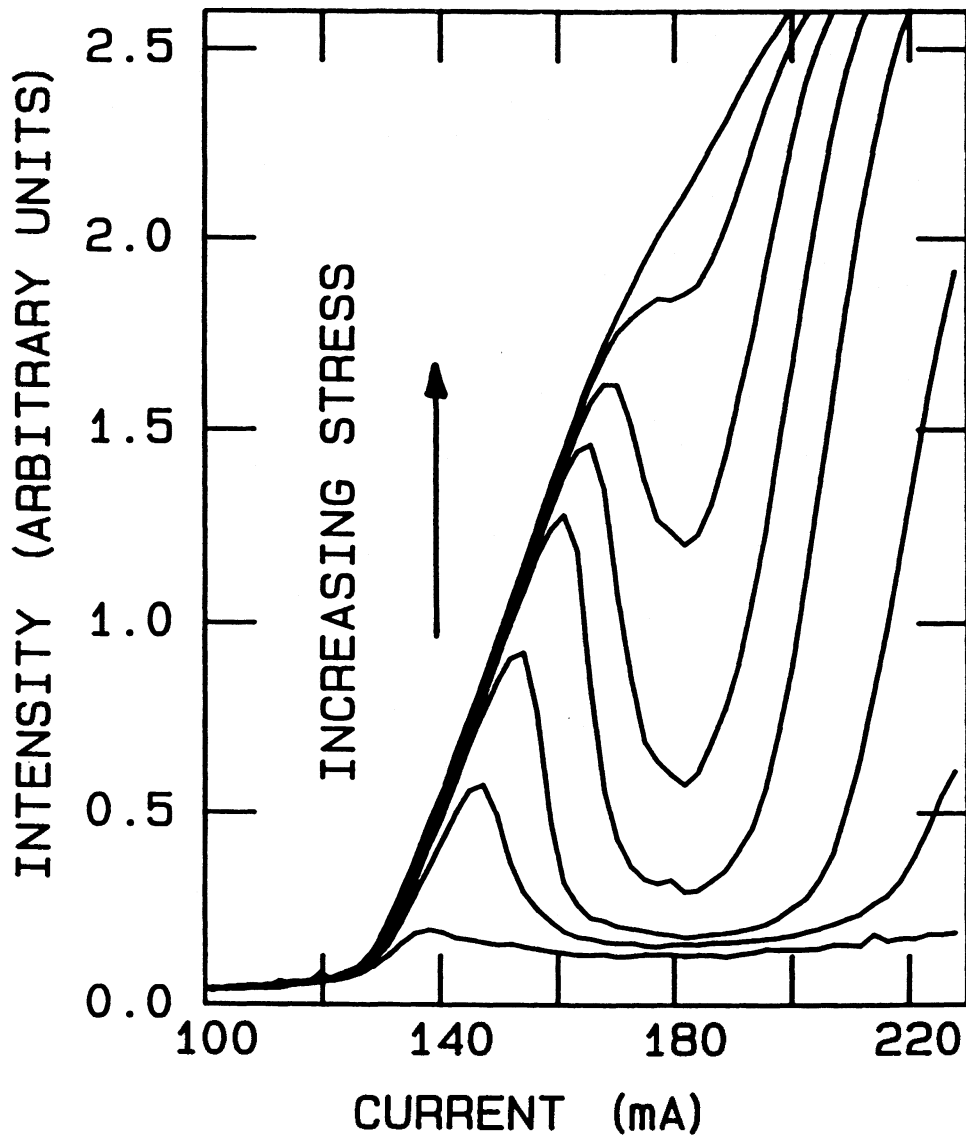


Figure 5.4:

Current and stress dependence of the TM mode intensity. The applied stress is increased in increments of $\Delta\sigma_x \sim 5 \times 10^5$ dyne/cm².

TE stimulated emission to a lower current (Fig. 5.5(b) curve 1). If the applied stress is adjusted, such that the TE and TM intensities are equal at the same current as before (Fig. 5.5(b) curve 2) then the mechanical stress change must be equal to the thermal stress produced in this time interval. The threshold increase is used to calculate the temperature change in the active region. The thermal stress change measured using this technique as a function of the temperature rise of the active region is shown in Fig. 5.5(a). The experiment was repeated ten times with the same laser to obtain a distribution of points and the error bars (one standard deviation) shown.

The solid line in Fig. 5.5(a) shows a theoretical relationship between the thermal stress and the temperature change in the active region. In this calculation it is assumed that the temperature of the device increases uniformly and therefore that the thermally induced stress results completely from the difference between the thermal expansion coefficients of the quaternary active layer and the InP cladding layers. This assumption is based on the analysis of the thermal response of gain-guided lasers reported by Nakwashi [42]. As the substrate is much thicker than the epitaxial layers, the stress within the active region due to a temperature increase ΔT is given by [9]

$$\Delta \sigma_x = \frac{E}{1-\nu} \frac{(t_s + 2t_c - 3t_a)}{t} \Delta \alpha \Delta T \quad (5.1)$$

where t_s , t_c , t_a , and t are the thicknesses of the substrate, the cladding layers, the active layer and the total thickness of the wafer respectively, $\Delta \alpha$ is the difference between the thermal expansion coefficients of InGaAsP and InP, E is Young's

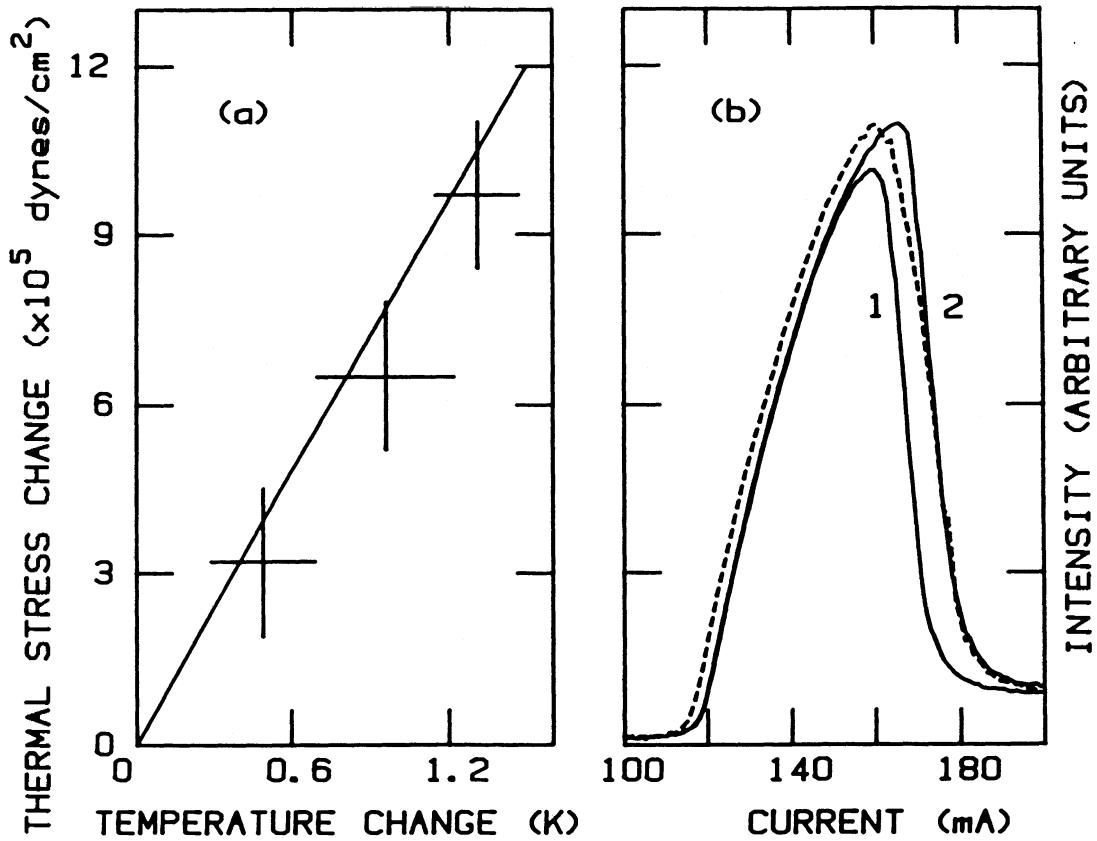


Figure 5.5: Measurement of the thermal stress using the polarization resolved LI -curve at a critical applied stress.

- (a) The solid curve shows the calculated thermal stress change in the active layer $\Delta\sigma_x$ produced by a temperature change ΔT . The experimental points are obtained by cancelling the thermal stress change with a mechanical stress using the polarized resolved LI -curves at the critical stress as shown in (b).

modulus and ν is Poisson's ratio. With $t_s = 100 \mu\text{m}$, $t_c = 3 \mu\text{m}$, $t_a = 0.2 \mu\text{m}$, $\Delta\alpha = 0.81 \times 10^{-6} / ^\circ\text{C}$, $E = 6.1 \times 10^{11} \text{ dyne/cm}^2$, and $\nu = 0.341$, equation (5.1) becomes,

$$\Delta\sigma_x = 8 \times 10^5 \Delta T \text{ (dyne/cm}^2\text{)} \quad (5.2)$$

It is apparent from Fig. 5.5(a) that there is a good agreement between the measured thermal stress and the value expected from equation (5.2).

The thermal stress induced by current heating over a $1 \mu\text{s}$ time scale is of order 10^6 dyne/cm^2 . This stress is three orders of magnitude smaller than the applied stresses required to cause significant changes in the wavelength and threshold of the laser. The possibility of measuring stress variations on the scale of 10^5 dyne/cm^2 illustrates the sensitivity of the polarization behaviour at the critical applied stress. This effect could be used to develop an instrument which is extremely sensitive to small forces or accelerations.

5.3 Polarisation of the spontaneous emission.

The results of *Chapter 4* and *Section 5.1* and *5.2* were concerned with the effects of stress on the above threshold behaviour of semiconductor diode lasers. In this section the below threshold behaviour will be discussed.

Below threshold the light output is a mixture of spontaneous emission and amplified spontaneous emission. If the active region is completely stress-free the polarisation of the spontaneous emission will be isotropic [43]. Also, the gains of the TE and the TM modes are equal in a stress free laser (see *Section 3.2*), therefore the

polarisation of the amplified spontaneous is isotropic. As the TE mode reflectivity is larger than the TM mode reflectivity [38], the threshold condition for the TE mode will be satisfied, but the TM mode remains lossy. At the TE threshold, the TM power saturates and the excess inversion is channelled into the TE mode. This saturation of the TM mode intensity at threshold was measured for a PBH laser. The results are plotted in Fig. 5.6. It can be seen that, below threshold, the intensities of TE and TM polarised light are approximately equal. Another way of looking at the results of Fig. 5.6 is to plot the degree of polarisation ρ as a function of current. The degree of polarisation is defined by

$$\rho = \frac{I_{\text{TE}} - I_{\text{TM}}}{I_{\text{TE}} + I_{\text{TM}}} \quad (5.3)$$

where I_{TE} and I_{TM} are the intensities of the TE and TM polarised light. If the active region is stress-free then, below threshold $I_{\text{TE}} = I_{\text{TM}}$ and $\rho = 0$. Above threshold I_{TM} saturates therefore $I_{\text{TE}} \gg I_{\text{TM}}$ and $\rho \sim 1$.

What happens to the degree of polarisation when the lattice within the active region is deformed by stress? A compressive strain increases the probability of emission of photons which are polarised parallel to the strain direction (see *Section 3.2*). As a result the degree of polarisation below threshold depends on the stress distribution within the active region of the laser.

The degree of polarisation at different values of the applied stress was investigated for six buried heterostructure lasers and six stripe geometry DH lasers. It was found that the buried heterostructure lasers studied have a degree of

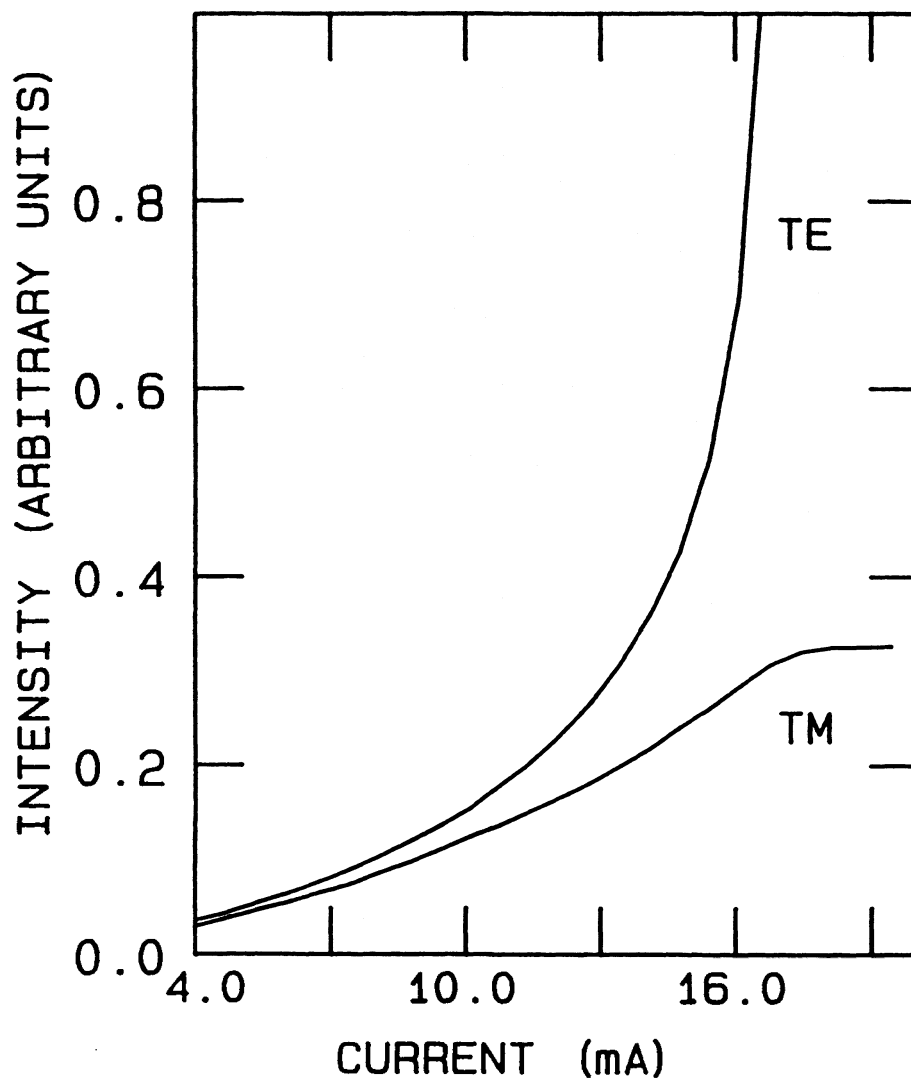


Figure 5.6: Polarization resolved *LI*-curve of a PBH laser. Shown here is the saturation of the TM mode at threshold.

polarisation with no applied stress at low currents of $\rho \sim 10\%$, in favour of TE polarised light. This implies that there is an internal stress within the active region which favours the emission of TE polarised photons. Using the theory presented in *Section 3.2* it follows that the internal stress must be either compressive and parallel to the junction plane, or tensile and perpendicular to the junction plane. The effect of this internal stress can be cancelled with an applied stress as shown in Fig. 5.7(a). With no applied stress the degree of polarisation at low current is $\sim 10\%$. The degree of polarisation increases abruptly to $\sim 100\%$ above ~ 17 mA, which corresponds to the lasing threshold of the diode. By applying a tensile stress parallel to the junction plane, $\sigma_x \sim 1.1 \times 10^9$ dyne/cm², the degree of polarisation at low current is reduced to zero. This suggests that under this applied stress there is no net strain within the active region. The increase in threshold caused by the applied stress can be seen in Fig. 5.7(a).

In *Section 4.1*, it was suggested that an internal stress which favoured the TE mode could explain why the buried heterostructure lasers studied do not switch to the TM mode even with an applied stress upto 4×10^9 dyne/cm². This hypothesis is supported by the below threshold behaviour.

The stripe geometry DH lasers which were discussed in *Section 4.1* show a transition to TM polarised stimulated emission at a relatively low applied stress, $\sigma_x \sim 1 \times 10^9$ dyne/cm². In this case it is expected that the fabrication stress would favour the emission of TM polarised photons. The current dependence of the degree of polarisation of a laser typical of this wafer is shown in Fig. 5.7(b). At low current, and with no applied stress the degree of polarisation is $\sim -15\%$. This implies that there is a fabrication stress within the active region which favours the TM mode.

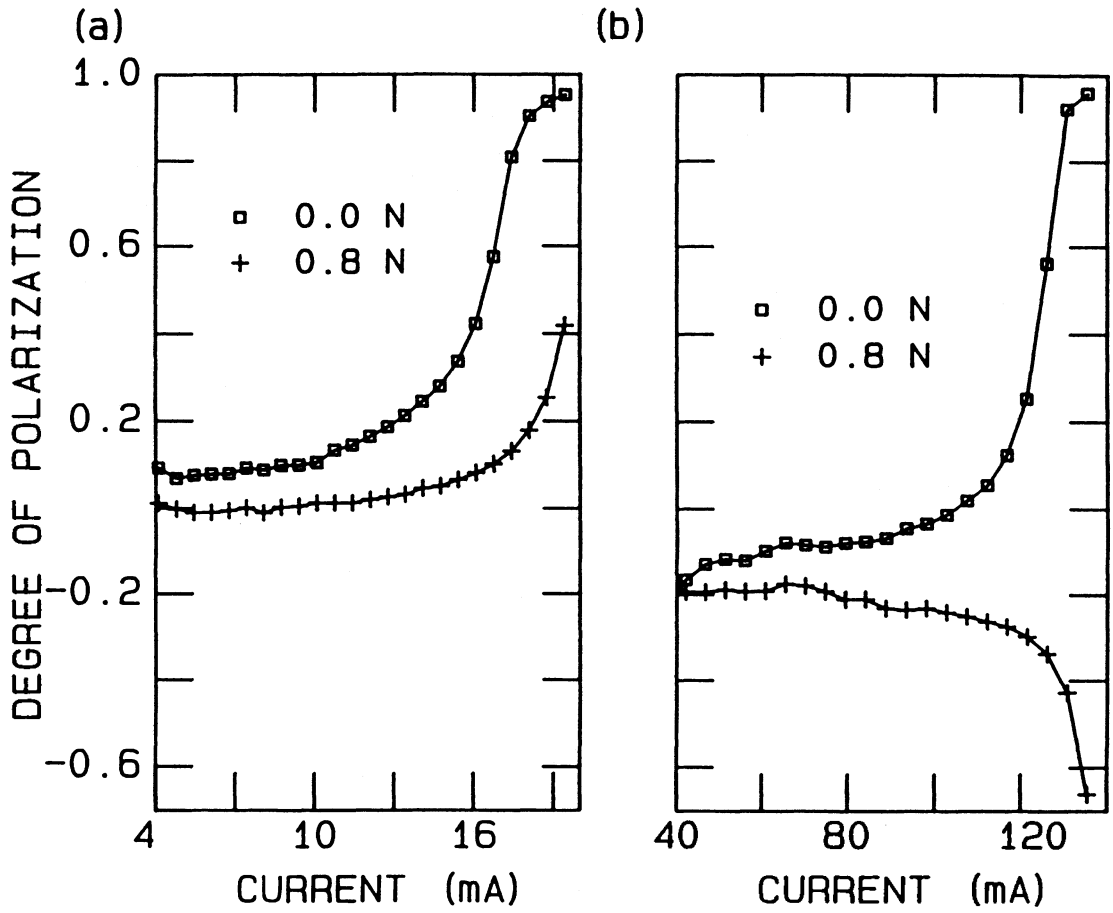


Figure 5.7:

Degree of polarization of (a) a PBH laser and, (b) a stripe geometry DH laser. The effect of the applied stress on the degree of polarization is shown: No applied stress (\square) and $\sigma_x \sim 1.1 \times 10^9$ dyne/cm² (+).

This result is expected if the low critical applied stress values measured in *Section 4.1* are due to internal stress. It is interesting to note that even though more TM polarised photons are emitted below threshold the device still lases in the TE mode. This is because of the difference in the reflectivities of the TE and the TM mode. In a gain-guided laser the TE mode reflectivity is $\sim 15\text{--}20\%$ larger than the TM mode reflectivity [38]. This means that the TM mode gain must be $\sim 15\text{--}20\%$ larger than the TE mode gain for the laser to operate in the TM mode. This effect should be observed in the degree of polarisation below threshold with the applied stress set above the transition to the TM mode. As shown in Fig. 5.7(b) a degree of polarisation below threshold of $\sim -20\%$ is required to give lasing in the TM mode.

The degree of polarisation of some reject buried heterostructure was also investigated. Usually, the buried heterostructure lasers in this study have thresholds in the range $15\text{--}20\text{ mA}$. The reject lasers if they lase have thresholds in excess of 50 mA . It was thought that the reason why the thresholds of these devices are so high could be due to a large internal stress within the active region. The degree of polarisation of a typical reject buried heterostructure laser is shown in Fig. 5.8. The degree of polarisation below threshold is $\sim 40\%$. This suggests an extreme internal strain which could explain the high threshold of 70 mA . A similar result was obtained with three other reject PBH lasers.

It is possible that by operating a laser at high current and high temperature, the defects and dislocations in the device will obtain enough energy to diffuse through the crystal and therefore alter the stress distribution. Such changes in the internal stress could be related to the threshold and efficiency variations, which are observed during the aging of semiconductor diode lasers. If the internal stress

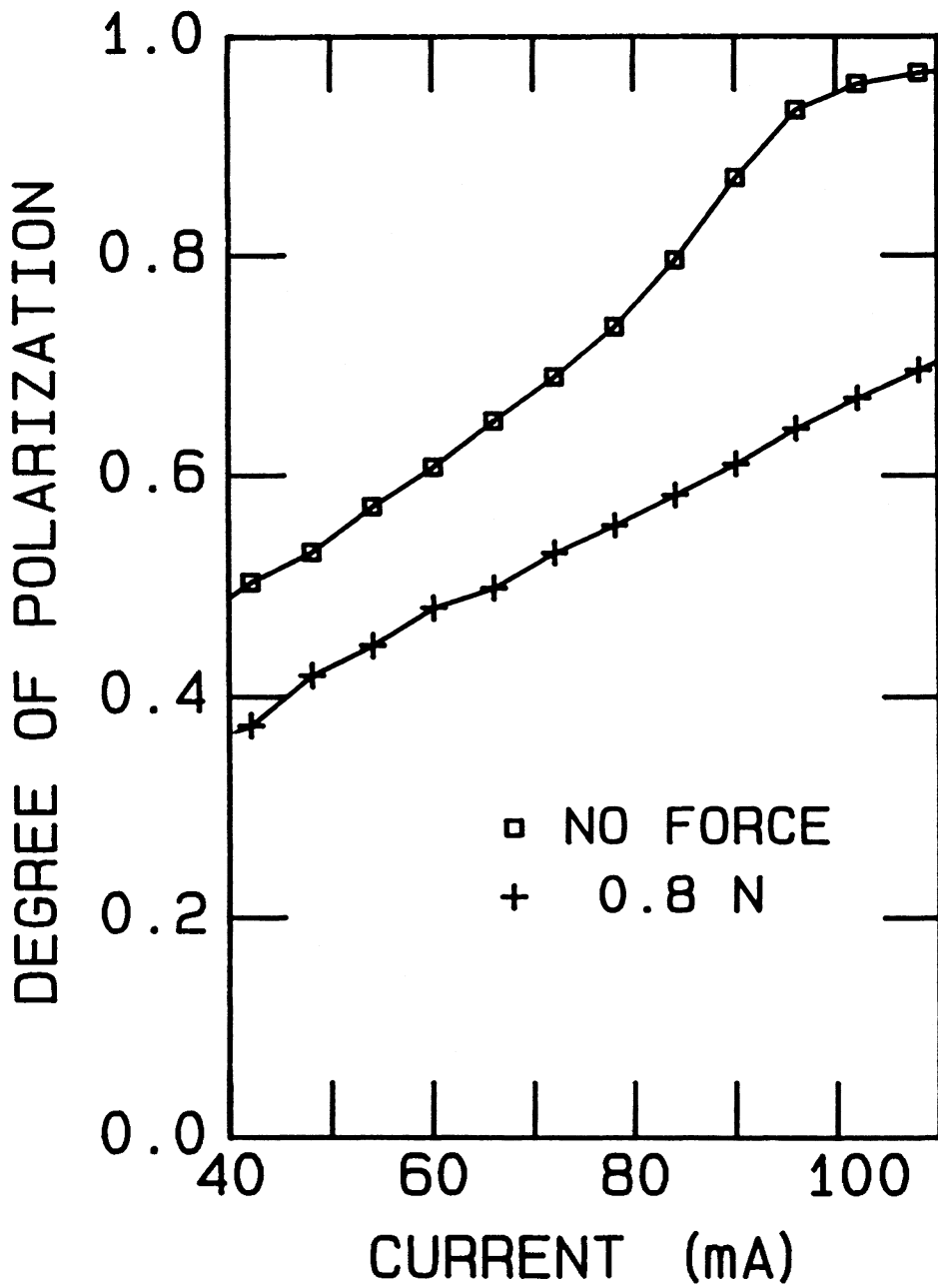


Figure 5.8:

Degree of polarization of a reject PBH laser. With no applied stress, at low current $\rho \sim 40\%$. Threshold is ~ 70 mA.

does change during aging this should show up in the degree of polarisation of the spontaneous emission. A preliminary investigation of the relationship between the polarisation behaviour below threshold and degradation of the laser was made. After operating a stripe geometry DH laser for 16 hours at 230 mA, the threshold current increased by 6 % and the degree of polarisation of the spontaneous decreased by ~ 2 %. This is an isolated result and further investigation of this phenomenon is needed.

5.4 Summary.

In *Section 5.1* the effect of current and temperature on the polarisation of the output of lasers biased at the critical applied stress was investigated. It was found that the polarisation of the output switched from TE to TM or *vice versa* as the current was varied. This switching was explained by the current-induced thermal stress. From the polarisation resolved *LI*-curve at the critical applied stress it was concluded that the direction of the current-induced thermal stress is different in the PBH and stripe geometry DH structures.

The sensitivity of the polarisation of the output at the critical stress to small changes in the stress distribution was used to measure the current-induced thermal stress (*Section 5.2*). The thermal stress change in the active layer caused by a $1 \mu\text{s}$ current pulse was measured and found to be $\sim 10^6$ dyne/cm².

In *Section 5.3* the strain dependent behaviour of the lasers below threshold was discussed. The results of measurements of the stress dependence of the degree of polarisation of the spontaneous emission were found to be consistent with the strain

dependence of the TE and TM mode gains and the TE and TM mode reflectivities. The degree of polarisation of the spontaneous emission was shown to be a useful indicator of the strain (internal or applied) in the active region of the device.

In *Chapter 6* the conclusions are discussed and some suggestions of possible extensions of this work are considered.

CHAPTER 6.

CONCLUSION.

By producing a bending stress in unbonded InGaAsP semiconductor diode laser chips it was possible to study the effects of tension and compression on the performance of the device. The relationship between threshold, wavelength and the polarization of the laser output and the applied stress has been investigated. The stress dependence of threshold and the transition to TM polarised stimulated emission when a tensile stress is produced in the active region is consistent with the theoretical expressions for the TE and TM mode gains derived in *Chapter 3*. The variation of the wavelength with stress is shown to be consistent with the energy splitting of the light- and heavy-hole band caused by the deformation.

The far-field distribution of the laser was unaffected by the applied bending. This result is expected from the stress calculation which shows that the variation of the applied stress across the active region is not sufficient to produce photoelastic guiding of the lasing mode.

The effect of the stress distribution produced by the contact on the operating characteristics of the lasers was investigated. It was found that the contact stress produced different behaviour from the bending moment. For example, the contact stress caused a rotation of the plane of polarisation of the stimulated emission, whereas the bending stress induced an abrupt transition from TE to TM polarised stimulated emission. It was found that the contact stress produced an increase in the maximum output power of stripe geometry DH lasers. It is thought that this effect maybe caused by photoelastic guiding.

At a critical stress the polarization of the stimulated emission changes from TE to TM. The magnitude of this critical stress varies from wafer to wafer. It was suggested that the value of the critical applied stress could be related to the fabrication stress in the active region.

The effect of current on the polarization with the laser operated at the critical applied stress was investigated. It was found that current produces a switching between the TE and TM modes. This switching can be explained in terms of the current-induced thermal stress in the active region. The effect of the current-induced stress was opposite in the buried heterostructure and stripe geometry double heterostructure lasers studied. This result is attributed to the structural differences. A comparison of the polarisation resolved LI -curves of stripe geometry DH lasers with InP and InGaAsP confining layers shows that the layer composition has a significant effect on the thermal stress.

The sensitivity of the polarization to small variations of stress is used to measure the current-induced stress. It is found that these thermal stresses are $\sim 10^5$ dyne/cm² which is four orders of magnitude smaller than that required to produce significant changes in the laser wavelength or threshold. A good agreement between the measured thermal stress and a theoretical value calculated from the thermal expansion of the active layer was obtained.

The effect of stress on the below threshold behaviour of the lasers was studied. The results show that compressive stress increases the intensity of spontaneous emission polarised parallel to the stress direction. The polarisation of the spontaneous emission with no applied stress of most of the lasers examined was not isotropic. This result indicates that there is an internal stress within the active

region. These results are consistent with the value of the critical applied stress measured in *Section 4.1* which is also related to the internal strain.

In previous work only the effects of uniaxial compression stress on the operating characteristic of semiconductor diode lasers has been studied. In this work both compression and tension have been investigated and the results are compared to the effect of the stress distribution caused by the contact. These measurements have improved our understanding of how strain affects the lasing characteristics. This knowledge has enabled us to provide a more complete theoretical description of the stress dependence of optical gain in semiconductors.

The contact stress produced some interesting results especially shifting the roll-off of gain-guided lasers to higher output powers. This area offers a possibility for future work. If the profile of the probe is known accurately then the Hertzian stress distribution could be calculated. Or one could work backwards from the stress distribution required to produce a photoelastic waveguide, to the desired profile for the probe. The use of a probe to induce a localised stress, provides a technique to investigate the effect of an anisotropic stress distribution. This technique has more freedom than using uniaxial stress and could add significantly to the understanding of the physics of operation of semiconductor diode lasers.

At a critical applied stress the lasers appear to oscillate in the TE and TM modes simultaneously. However, it is possible that the output is oscillating between polarisation modes on a time scale which is too fast for the measurement system. It may be interesting to examine the intensity of each polarisation mode on a hundred picosecond time scale. If the output is oscillating between modes, then what is the frequency spectrum of these oscillations ?

At the critical applied stress a small change in the active region temperature or the current resulted in switching between polarisation modes. It is thought that feedback of the spontaneous emission of the polarisation mode which is not lasing could induce a transition to lasing in that mode.

In *Section 5.3*, a preliminary investigation of the relationship between the polarisation of the spontaneous emission and degradation of the laser was discussed. This experiment should be repeated for more lasers. Also, it would be interesting to age the device with the active region under tension and then under compression and measure the effect on the internal stress distribution.

If a semiconductor diode laser is subject to an applied stress a threshold change is observed. However it was not certain what mechanism is responsible for the threshold change. In this work it has been shown that the threshold changes can be explained using a model based on the strain dependence of the valence band wavefunctions. The effects of stress on the wavelength of emission and the polarisation of the output above and below threshold were measured and the results are explained in terms of the same model. Some other interesting stress related phenomena were observed. These include an increase in the peak output of stripe geometry DH lasers which is thought to be caused by photoelastic guiding and current-induced polarisation switching at a critical applied stress. These effects open up the possibility for further work in this area.

APPENDIX A.
LASER DRIVER CIRCUIT.

A circuit diagram of the laser driver is shown in Fig. A1. The laser is connected in one arm of a differential pair which forms the load of a constant current source. The current through the laser is pulsed by the TTL inputs supplied to the base of the switching transistors T_1 (Motorola MPS 3646). The rise time, for a current pulse of amplitude 230 mA is less than 10 ns and is limited by the rise time of the TTL pulse. The TTL inputs are terminated with 50Ω to ground to avoid ringing. To reduce ringing on the current pulse, the connections to the laser have to be short (< 10 cm).

The constant current source effectively operates d.c., as the current is always passing through one or other of the arms of the differential pair. This has the advantage that the constant current source does not have to switch large currents. However, as the impedance of the two arms of the differential pair are not equal, the emitter voltage on the transistor T_2 is not constant. The components in the current source must be able to respond to this voltage change. These components are:

Op-Amp:	RCA CA 3130E
Transistors T_2 , and T_3 :	Motorola 2N2222 A.

When the current through R_1 reach a particular value the voltage across R_1 is sufficient to turn T_3 on which limits the maximum current through the load.

The current can be calculated from the voltage across R_1 (10 Ω metal film resistor, 1% tolerance), or across R_2 (two 1 Ω metal film, 1%). To measure the voltage across R_1 requires a second boxcar integrator to capture the pulse. However,

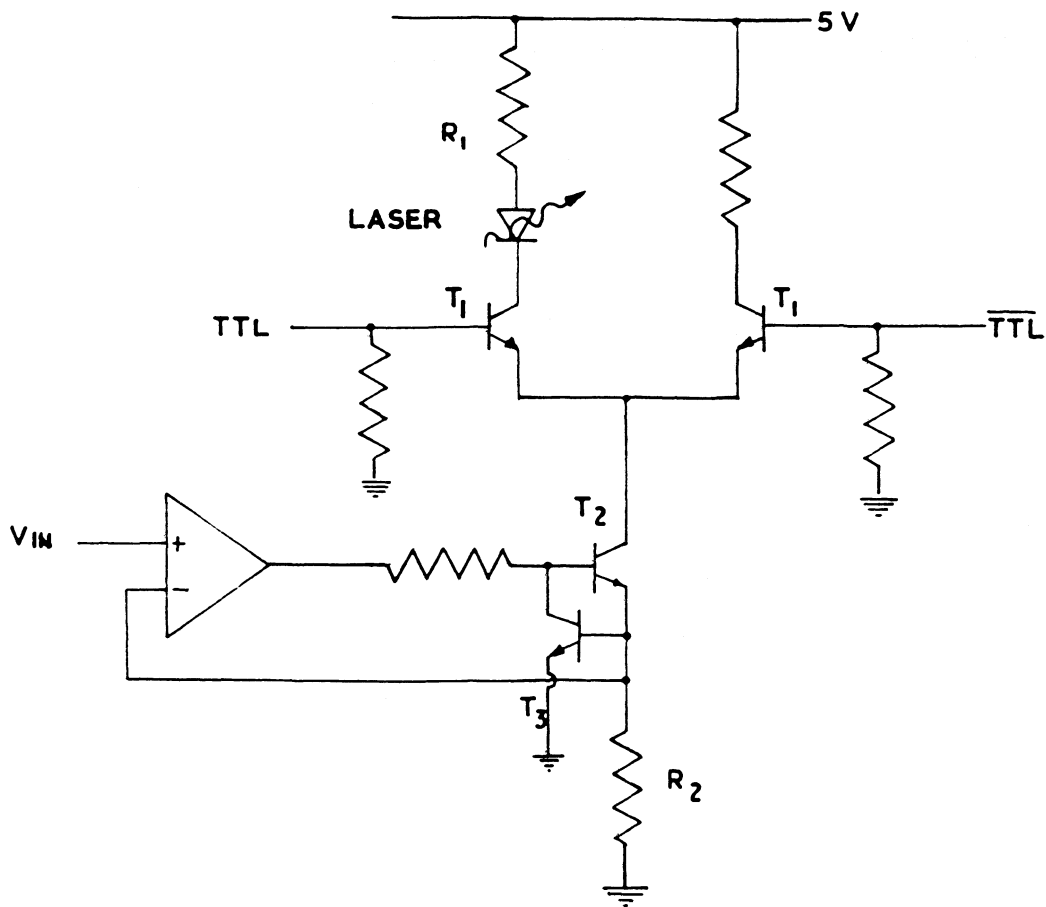


Figure A.1: Circuit diagram of the laser driver.

there is an accurate linear relationship between the current and the input voltage V_{in} . Therefore, it is not always necessary to measure the current directly.

The resistor (1 k Ω , 10%) between the output of the op-amp and the base of T₂ prevents the output of the op-amp from being shorted when T₃ turns on. Two 0.01 μ F (ceramic disc) capacitors are connected between the op-amp inputs and ground. Without these capacitors, the current does not go back to zero when $V_{in} \rightarrow 0$. There is a 2.2 nF (ceramic) compensation capacitor between pins 1 and 8 of the op-amp. There is a 68 μ F (electrolytic) capacitor between the supply and ground. This is a decoupling capacitor which supplies charge when it is needed. The circuit is built on copper plate board. The copper plate is used as the ground plane. It was found that using copper plated board gave a better pulse shape than printed circuit board.

APPENDIX B.

BOXCAR INTEGRATOR AND DATA ACQUISITION SYSTEM.

To neglect the thermal impedance between the laser chip and the heat-sink the measurements are made within the first 200 ns of each light pulse. The beginning of the pulse is noisy due to turn-on transients such as ringing on the current pulse. To avoid this region a programmable time delay circuit is used to open the gate of the boxcar integrator at a fixed time after the beginning of the pulse. The circuit has a minimum delay of 100 ns.

The boxcar integrator was supplied with an RC time constant of 100 μ s. This means that with an integration time of 100 ns (integrate one pulse) the output is equal to 0.1% of the input. To increase this signal the time constant was decreased to 1 μ s by replacing the integrating capacitor (10 μ F polystyrene) with a 100 nF polystyrene capacitor. As there is a long time between pulses (1 ms) and it is desirable to make many measurements in a short time, the total integration time is limited to a few time constants. To maximise the output the gate time must be as long as possible. The pulses are 200 ns long and there is a minimum delay of 100 ns therefore gate times of 100 ns are used.

The falling edge of the TTL pulse triggers the data acquisition system (MDAS) to measure the output of the boxcar. It was found that the initial readings made by the MDAS are in error. For this reason the data on the first ten pulses are ignored. The readings on the next ten pulses are stored and the average is sent to the computer. The integrator is not reset between readings, therefore the values stored in the computer are given by

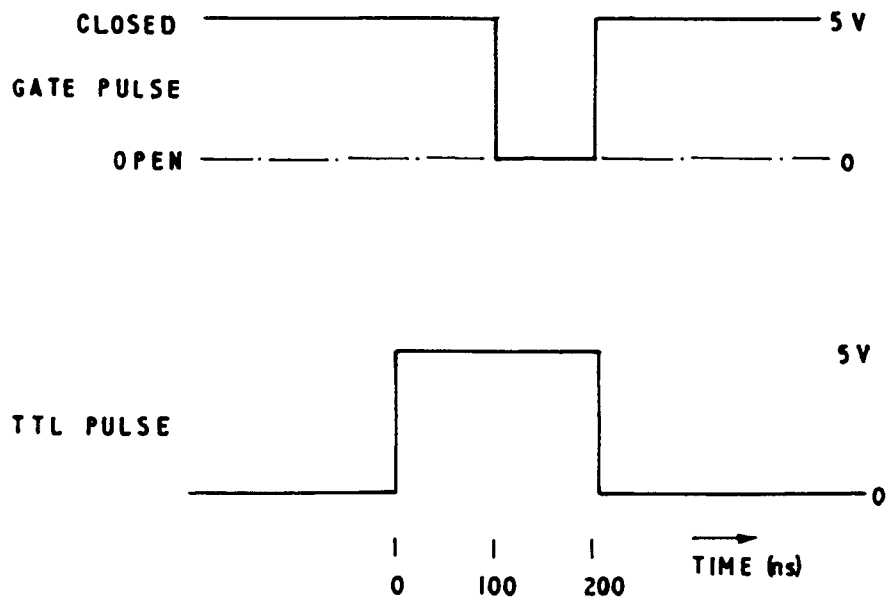


Figure B.1: Timing diagram for the measurement system.

$$V_1 + \frac{\Delta V}{10} \sum_{n=10}^{n=20} [1 - \exp(-n/10)] = V_1 + 0.78\Delta V \quad (\text{B.1})$$

where V_1 is the initial voltage on the boxcar and ΔV is the difference between V_1 and the new pulse amplitude. Using equation (B.1) the actual detector output can be obtained. The reset switch on the boxcar is not used because this would require a pulse counter and an additional TTL pulse driver to trigger the reset after every twenty pulses.


```

250 ON KEY 5 GOTO 2120      ! SAVE PREVIOUS DATA
260 ON KEY 7 GOTO 2250      ! SAVE THRESHOLD DATA
270 ON KEY 9 GOTO 1920      ! PLOT LI ON HPPLT
280 ON KEY 10 GOTO 650      ! RUN LI AND PLOT WITH PREVIOUS DATA
290 !
300 !
310 !
320 !
330 !
340 ! REM   ENTER INITIAL, FINAL CURRENT AND NUMBER OF POINTS
350 !
360 PRINT "Press c to reset default values."
370 INPUT KEY WAIT A$ | IF A$="c" THEN
380   INPUT PROMPT "Input start current." ALTER "000":Sc
390   INPUT PROMPT "Input number of data points." ALTER "100":Num
400   INPUT PROMPT "Input final current." ALTER "230":Fc
410   !       REM CONVERT CURRENT VALUES TO VOLTAGE ARRAY C
420   Start = (Sc-0.4)*0.04
425   Fini = (Fc-0.4)*0.04
430   Inc = (Fini-Start)/Num
440   DIM C1[Num/2],I[Num],L[Num],B[10],C2[Num/2],C[Num]
450   B = 0
460   C = ARY(Start,Inc)
470   ! REM       DEFINE ARRAY C TO RAMP CURRENT UP AND DOWN
480   ! C1 = ARY(Start,2*Inc)
485   ! C2 = ARY(Fini,-2*Inc)
490   ! FOR Q = 1 TO Num/2 | C[Q] = C1[Q] | NEXT Q
500   ! FOR Q = Num/2+1 TO Num | C[Q] = C2[Q-Num/2] | NEXT Q
510 END IF
520 !
530 !
540 !
550 !
560 !
570 ! REM                               PROGRAM EXECUTABLE BUFFER IN MDAS
580 CLEAR
590 PRINT AT 1,15:"LOAD MDAS (Y/N) ? ";
600 INPUT KEY WAIT A$
610 IF A$="Y" THEN
620   PRINT AT 1,15:"Loading MDAS"
630   GOSUB 1330
640 END IF
650 Times = Times+1
660 ! REM                               SET TRIGGER TYPE: FALLING EDGE OF TTL PULSE
670 PRINT #1:"tri 3 a4;"
680 ! REM                               ENABLE TRIGGER
690 PRINT #1:"wrch a4 32;"
700 ! REM                               SET BUFFERS 4 AND 5 TO ZERO
710 PRINT #1:"rd 4;" | PRINT #1:10,B

```

```

720 PRINT #1:"rd 5;" | PRINT #1:10,B
730 ! REM                                RUN EXECUTABLE BUFFER
740 PRINT AT 1,15:"Taking data."
750 FOR Q = 1 TO Num
755   PRINT #1:"RUN 10;"
760   INPUT #1:L[Q] | NEXT Q
765 NEXT Q
767 ! REM                                CONVERT LIGHT DATA TO MILLIWATTS
770 L = -L/0.435
780 ! REM                                SET-UP GRAPH
790 IF Times=1 THEN | GOSUB 2400 | END IF
800 Top = Lmax-Lmax/2
810 ! REM                                RESET CURRENT
820 PRINT #1:"sas a7",C[1],";"
830 ! REM                                DISABLE TRIGGER
840 PRINT #1:"wrch a4 0;"
850 SET POINT STYLE 7
860 ! REM                                DEFINE CURRENT IN TERMS OF OUTPUT VOLTAGE
870 I = C/0.04+0.5
880 I = ROUND(I,1)
890 ! REM                                PLOT LI-CURVE
900 PLOT LINE I,L
910 !
920 !
930 !
940 !
950 !
960 ! REM                                STRAIGHT LINE FIT (SLF)
970 !
980 ! REM                                SET UPPER AND LOWER LIGHT VALUES FOR SLF
990 Ilow = 0.2 | Iup = 1.0
1000 ! INPUT ALTER "0.2,0.8":Ilow,Iup
1010 PRINT AT 1,15:"          "
1020 Q = 1
1030 DO WHILE L[Q]<Ilow | Lower = Q | Q = Q+1 | LOOP
1040 DO WHILE L[Q]<Iup | Q = Q+1 | Upper = Q | LOOP
1050 N = Upper-Lower
1060 IF N<3 THEN | PRINT "Less than three points in linear fit !"
1070 GOTO 2170 | END IF
1080 DIM X[N],Y[N],Xx[N],Xy[N]
1090 FOR Q = 1 TO N
1095   X[Q] = I[Lower+Q-1] | Y[Q] = L[Lower+Q-1] | NEXT Q
1100   Xx = X*X | Xy = X*Y
1110   Delta = N*SUM(Xx)-SUM(X)^2
1120   Slope = (N*SUM(Xy)-SUM(X)*SUM(Y))/Delta
1130   Yinte = (SUM(Xx)*SUM(Y)-SUM(X)*SUM(Xy))/Delta
1140   Xinte = -Yinte/Slope
1150 ! REM                                THRESHOLD EQUALS X-INTERCEPT
1160 Ith[Times] = Xinte

```

```

1170 Ith[Times] = ROUND(Ith[Times],1)
1180 Labx = Xmin+(Xmax-Xmin)*0.1 ; Laby=(Ymax-Ymin)*0.9-4*Times*Yunit
1190 TEXT AT Labx,Laby:"Ith";Times;" = ";Ith[Times];"mA"
1200 Inter = (I[Upper]-I[Lower])/N
1210 X = ARY(I[Lower],Inter)
1220 Y = Slope*X+Yinte
1230 ! REM                                PLOT STRAIGHT LINE
1240 PLOT X,Y
1250 INPUT KEY WAIT Q$
1260 SET DIALOG | STOP
1270 !
1280 !
1290 !
1300 !
1310 !
1320 ! REM                                LOAD MDAS
1330 OPEN #1:"com1:";"f"
1340 ! REM                                OUTPUT INITIAL CURRENT
1350 PRINT #1:"sas a7",C[1];;"
1360 ! REM                                DEFINE 5 FLOATING POINT BUFFERS
1370 ! REM                                BUFFER 1 FOR OUTPUT VOLTAGE
1380 ! REM                                BUFFER 3,5 FOR LIGHT DATA
1390 ! REM                                BUFFER 2,4 FOR CURRENT DATA
1400 PRINT #1:"dfn 1 201 4 2 11 4 3 11 4;"
1410 PRINT #1:"dfn 4 11 4 5 11 4;"
1420 ! REM                                DEFINE EXECUTABLE BUFFER
1430 PRINT #1:"dfn 10 1000 5;"
1440 ! REM                                READ OUTPUT VOLTAGE C INTO BUFFER 1
1450 PRINT #1:"rd 1;"
1460 PRINT #1:Num,C
1470 ! REM                                PROGRAM EXECUTABLE BUFFER
1480 PRINT #1:"load 10;"
1490 ! REM                                OUTPUT VOLTAGE FROM BUFFER 1 TO CHANNEL A7
1500 PRINT #1:"aofs a7 1;"
1510 ! REM                                READ INPUT ON CHANNEL D1 AND DUMP IN BUFFER 6
1520 ! REM                                REPEAT 10 TIMES
1530 PRINT #1:"ai 10 d1 6 1;"
1540 ! REM                                READ INPUT ON D1 AND STORE IN BUFFER 3
1550 PRINT #1:"ai 1 d1 3 16;"
1560 ! REM                                ADD BUFFERS 3 AND 5
1570 PRINT #1:"add 3 5 5;"
1580 ! REM                                REPEAT 10 TIMES
1590 PRINT #1:"ai 1 d1 3 16;"
1600 PRINT #1:"add 3 5 5;"
1610 PRINT #1:"ai 1 d1 3 16;"
1620 PRINT #1:"add 3 5 5;"
1630 PRINT #1:"ai 1 d1 3 16;"
1640 PRINT #1:"add 3 5 5;"
1650 PRINT #1:"ai 1 d1 3 16;"

```

```

1660 PRINT #1:"add 3 5 5;"
1670 PRINT #1:"ai 1 d1 3 16;"
1680 PRINT #1:"add 3 5 5;"
1690 PRINT #1:"ai 1 d1 3 16;"
1700 PRINT #1:"add 3 5 5;"
1710 PRINT #1:"ai 1 d1 3 16;"
1720 PRINT #1:"add 3 5 5;"
1730 PRINT #1:"ai 1 d1 3 16;"
1740 PRINT #1:"add 3 5 5;"
1750 PRINT #1:"ai 1 d1 3 16;"
1760 PRINT #1:"add 3 5 5;"
1770 ! REM          SEND DATA IN BUFFER 5 TO COMPUTER
1780 PRINT #1:"ave 5;"
1790 ! REM          RESET BUFFER 5 TO ZERO
1800 PRINT #1:"neg 5 3;"
1810 PRINT #1:"add 3 5 5;"
1820 PRINT #1:"end;"
1830 RETURN
1840 !
1850 !
1860 !
1870 !
1880 !
1890 ! REM          CONTROL CURRENT FROM KEYBOARD
1900 SET DIALOG
1910 OPEN #1:"com1:", "f"
1920 PRINT "Press A (increase) or Z (decrease) current"
1930 PRINT "or enter integer; current = 25 x integer"
1940 INPUT KEY WAIT A$
1950 IF A$="a" THEN | A = A+0.01 | GOTO 1990 | END IF
1960 IF A$="z" THEN | A = A-0.01 | GOTO 1990 | END IF
1970 IF A$=" " THEN GOTO 2020
1980 A = VAL(A$)
1990 PRINT #1:"sas a7",A, ";"
2000 li = 25*A
2010 PRINT AT 10,10:"I = ";li,"mA          "
2020 GOTO 1940
2030 SET DIALOG
2040 STOP
2050 !
2060 !
2070 !
2080 !
2090 !
2100 ! REM          SAVE LI DATA ON DISK IN B: DRIVE
2110 !
2120 INPUT PROMPT "Number of file ?":Aa$
2130 A$ = "b:" & Day$ & Aa$ & ".dat"
2140 OPEN #2:A$,"f"

```

```

2150 PRINT #2:Num,I,L
2160 GOTO 1250
2170 RETURN
2180 INPUT KEY WAIT Q$
2190 !
2200 !
2210 !
2220 !
2230 !
2240 ! REM                               SAVE THRESHOLD DATA
2250 Number = Times | DIM P[Number]
2260 FOR Q = 1 TO Number
2270   P[Q] = Ith[Q]
2280 NEXT Q
2290 Vietnam$ = "B:" & Laser$ & Laser$ & Laser$ & ".DAT"
2300 OPEN #2:Vietnam$,"F"
2310 PRINT #2:Number,P
2320 CLOSE #2
2330 !
2340 !
2350 !
2360 !
2370 !
2380 ! REM                               SUB-ROUTINE TO SET-UP GRAPH
2390 !
2400 CALL P_MAX(L,Lmax,Pmax) | CALL P_MIN(L,Lmin,Pmin)
2410 Ymin = ROUND(Lmin,0) | Ymax = ROUND(Lmax*1.1,1)
2420 CALL P_MAX(I,Imax,Pimax) | Xmax = ROUND(Imax*1.1,1)
2430 CALL P_MIN(I,Imin,Pimin) | Xmin = ROUND(Imin,0)
2440 Xmin = 100 | Xmax = 200
2450 X1v = 82 | X2v = 134 | Y1v = 14 | Y2v = 94
2460 SET VIEWPORT X1v,X2v,Y1v,Y2v
2470 SET WINDOW Xmin,Xmax,Ymin,Ymax
2480 Xunit = (Xmax-Xmin)/(X2v-X1v) | Yunit = (Ymax-Ymin)/(Y2v-Y1v)
2490 Xtext = 2.5*Xunit | Ytext = 2.5*Yunit
2500 Multext = Xtext/Ytext
2510 IF H$="Y" THEN | SET TEXT STYLE 0 | SET TEXT SIZE Ytext,1
2520 ELSE
2530   SET TEXT STYLE -1 | SET TEXT SIZE Ytext,Multext
2540 END IF
2550 Xint = (Xmax-Xmin)/6 | Yint = (Ymax-Ymin)/5
2560 Lxint = LOG10(Xint) | Lxint = INT(Lxint)
2570 Lyint = LOG10(Yint) | Lyint = INT(Lyint)
2580 Xint = Xint/10^Lxint | Xint = ROUND(Xint,0)*10^Lxint
2590 Yint = Yint/10^Lyint | Yint = ROUND(Yint,0)*10^Lyint
2600 SET CLIP
2610 FOR Q = 0 TO 8 | MOVE Xmin+Q*Xint,Ymin
2620   DRAW Xmin+Q*Xint,Ymin+4*Yunit
2630 NEXT Q

```

```

2640 FOR Q = 1 TO 12 | MOVE Xmax,Q*Yint
2650   DRAW Xmax-4*Xunit,Q*Yint | NEXT Q
2660 FOR Q = 1 TO 13 | MOVE Xmin+Q*Xint,Ymax
2670   DRAW Xmin+Q*Xint,Ymax-4*Yunit | NEXT Q
2680 FOR Q = 1 TO 12 | MOVE Xmin,Q*Yint
2690   DRAW Xmin+4*Xunit,Q*Yint | NEXT Q
2700 SET CLIP OFF
2710 PLOT LINE Xmin,Ymin;Xmin,Ymax;Xmax,Ymax;Xmax,Ymin;Xmin,Ymin
2720 FOR Q = Xmin TO Xmax STEP 2*Xint | Qq = Q-5*Xunit
2730   TEXT AT Qq,Ymin-4*Yunit:Q | NEXT Q
2740 FOR Q = 0 TO Ymax STEP Yint | Qq = Q-1*Yunit
2750   TEXT AT Xmin-10*Xunit,Qq:Q | NEXT Q
2760 Ix = Xmin+(X2v-X1v)*0.2*Xunit | Iy = Ymin-10*Yunit
2770 TEXT AT Ix,Iy:"CURRENT (mA)"
2780 Intext = 1/Multext | Ly = Ymin+Yunit*10 | Lx = Xmin-Xunit*10
2790 IF H$="y" THEN | SET TEXT SIZE Ytext,1
2800 ELSE | SET TEXT SIZE Ytext,Intext | END IF
2810 SET TEXT ANGLE 90
2820 TEXT AT Lx,Ly:"INTENSITY (ARBITRARY UNITS)"
2830 Xtext = 1.5*Xunit | Ytext = 1.5*Yunit
2840 Multext = Xtext/Ytext
2850 SET TEXT ANGLE 0 | IF H$="Y" THEN | SET TEXT SIZE Ytext,1
2860 ELSE | SET TEXT SIZE Ytext,Multext | END IF
2870 RETURN

```

REFERENCES.

1. R.M. Ryan and R.C. Miller, "The effect of uniaxial strain on the threshold current and output of GaAs lasers", *Appl. Phys. Lett.* Vol. 3, No. 9 pp. 162–163, Nov. 1963.
2. N.B. Patel, J.E. Ripper and P. Brosson, "Behaviour of threshold current and polarization of stimulated emission of GaAs injection lasers under uniaxial stress", *IEEE J. Quantum Electron.* Vol. QE-9, No. 2, pp. 338–341, Feb. 1973.
3. T. Kobayashi and K. Sugiyama, "Effects of uniaxial stress on the double heterostructure lasers", *Jpn. J. Appl. Phys.*, Vol. 12, No. 9, pp. 1388–1392, Sept. 1973.
4. P.G. Eliseev, B.N. Sverdlov and N. Shokhudzhaev, "Reduction of threshold current of InGaAsP/InP heterolasers by unidirectional compression", *Sov. J. Quantum Electron.* Vol. 14, No. 8, pp. 1120–1121, Aug. 1984.
5. P.G. Eliseev, B.N. Sverdlov, I. Ismailov and N. Shokhudzhaev, "Influence of anisotropic deformation on the radiative characteristics of GaInAsP/InP injection lasers. I. Lasing threshold, polarization and Watt–Ampere characteristics", *Sov. J. Quantum Electron.*, Vol. 16, No. 8, pp. 1046–1050, Aug. 1986.
6. P.G. Eliseev, B.N. Sverdlov, I. Ismailov and N. Shokhudzhaev, "Influence of anisotropic deformation on the radiative characteristics of GaInAsP/InP injection laser. II. Spectral characteristics and discussion", *Sov. J. Quantum Electron.*, Vol. 16, No. 8, pp. 1051–1055, Aug. 1986.
7. G. H. B. Thompson, *Physics of Semiconductor Laser Devices*. Wiley, New York, 1980, ch. 1.
8. R. Rimpler and W. Both, "Thermally induced stress in GaAs/GaAlAs stripe laser diodes", *IEE Proceedings*, Vol. 134 Pt. J, No. 6, p. 323–325, Dec. 1987.
9. Y.C. Chen and J.M. Liu, "Temperature–dependent polarization behavior of semiconductor lasers", *Appl. Phys. Lett.* Vol. 45, No. 7, pp. 731–733, Oct. 1984.
10. J.M. Liu and Y.C. Chen, "Compensation of internal thermal stresses in InGaAsP/InP lasers for polarization stabilization", *IEEE J. Quantum Electron.* Vol. QE-21, No. 3, pp. 271–276, March 1985.
11. W.C. Dautremont–Smith and S.M. Woelfer, "Stresses in the InP/Ti/Pt and InP/SiO₂/Ti/Pt multilayer systems", *Appl. Phys. Lett.*, Vol. 47, No.

- 1, pp. 31–33, July 1985.
12. D. Akhmedov, N.P. Bezhan, N.A. Bert, S.G. Konnikov, V.I. Kuchinskii, V.A. Mishurnyi and E.L. Portnoi, "Effect of internal strain on the polarization of the emission in InP–InGaAsP heterojunction laser structures", *Sov. Tech. Phys. Lett.*, Vol. 6, No. 6, pp. 304–305, June 1980.
 13. S. Sakai, H. Shiraishi and M. Umeno, "AlGaAs/GaAs stripe laser diodes fabricated on Si substrates by MOCVD", *IEEE J. Quantum Electron.*, Vol. QE–23, No. 6, pp. 1080–1084, June 1987.
 14. V.A. Elyukhin, V.R. Kocharyan, E.L. Portnoi and B.S. Ryvkin, "Polarization of the emission in injection lasers", *Sov. Tech. Phys. Lett.*, Vol. 6, No. 6, pp. 307–308, June 1980.
 15. P.A. Kirby, P.R. Selway and L.D. Westbrook, "Photo–elastic waveguides and their effect on stripe geometry GaAs/Ga_{1-x}Al_xAs lasers", *J. Appl. Phys.*, Vol. 50, No. 7, pp. 4567–4579, July 1979.
 16. N.K. Dutta and D.C. Craft, "Effect of stress on the polarization of stimulated emission from injection lasers", *J. Appl. Phys.*, Vol. 56, No. 1, pp. 65–70, July 1984.
 17. V. Swaminathan, W.R. Wagner, P.J. Anthony, G. Henein and L.A. Koszi, "Bonding pad induced stresses in (Al,Ga)As double heterostructure lasers", *J. Appl. Phys.*, Vol. 54, No. 7, pp. 3763–3768, July 1983.
 18. E. Yablonovitch and E.O. Kane, "Reduction of lasing threshold current density by the lowering of the valence band effective mass", *IEEE/OSA J. Lightwave Technol.* Vol. LT–4, No. 5, pp. 504–506, May 1986.
 19. N.K. Dutta, "Effects of uniaxial stress on optical gain in semiconductors", *J. Appl. Phys.* Vol. 55, No. 2, pp. 285–288, Jan. 1984.
 20. A.R. Adams, D. Patel, P.D. Greene and G.D. Henshall, "Influence of pressure on temperature sensitivity of Ga_xIn_{1-x}As_yP_{1-y} lasers", *Electron. Lett.*, Vol. 18, No. 21, pp. 919–920, Oct. 1982.
 21. A.P. Mozer, S. Hausser and M.H. Pilkuhn, "Quantitative evaluation of gain and losses in quaternary lasers", *IEEE J. Quantum Electron.* Vol. QE–21, No. 6, pp. 719–725, June 1985.
 22. H. Hasegawa, "Theory of cyclotron resonance in strained silicon crystals", *Phys. Rev.*, Vol. 129, No. 3., pp. 1029–1040, Feb. 1963.
 23. F.H. Pollak and M. Cardonna, "Piezo–electroreflectance in Ge, GaAs and Si", *Phys. Rev.*, Vol. 172, No. 3, pp 816–837, Aug. 1968.
 24. M. Chandrasekhar and F.H. Pollak, "Effects of uniaxial stress on the

- electroreflectance spectrum of Ge and GaAs", *Phys. Rev. B.*, Vol, 15, No. 4, pp. 2127–2144, Feb. 1977.
25. X.Z. Lu, R. Garuthara, S. Lee and R.R. Alfano, "Gallium arsenide photoluminescence under picosecond–laser–driven shock compression", *Appl. Phys. Lett.*, Vol. 52, No. 2, pp. 93–95, Jan. 1988.
 26. C.P. Kuo, S.K. Vong, R.M. Cohen and G.B. Stringfellow, "Effect of mismatch strain on bandgap in III–V semiconductors", *J. Appl. Phys.*, Vol. 57, No. 12, pp. 5428–5432, June 1985.
 27. P. Melman and W.J. Carlsen, "Interferometric measurement of time–varying longitudinal cavity modes in GaAs diode lasers", *Appl. Op.*, Vol. 20, No. 15, pp 2694–2697, Aug 1981.
 28. Y. Horikoshi, Chapter 15 in *GaInAsP alloy semiconductors*, ed. T.P. Pearsall, Wiley, New York 1982.
 29. J.K. Butler, "The effect of junction heating on laser linearity and harmonic distortion" in *Semiconductor devices for optical communications*, ed. H. Kressel, Springer–Verlag, Heidelberg 1980.
 30. W.B. Morton and L.J. Close, "Notes on Hertz's Theory of the Contact of Elastic Bodies", *Phil. Mag. S.6*, Vol. 43, No. 254, pp 320–329, Feb. 1922.
 31. J.E. Nye, *Physical Properties of Crystals*, Oxford, New York 1957.
 32. S. Timoshenko and S. Woinowsky–Krieger, *Theory of Plates and Shells*, McGraw–Hill, New York 1965.
 33. M.A. Eisenberg, *Introduction to the Mechanics of Solids*, Addison–Wesley, Reading, Mass. 1980.
 34. A.E.H. Love, *A Treatise on the Mathematical Theory of Elasticity*, Dover, New York, 1927.
 35. E.O. Kane, "Band Structure of Indium Antimonide", *J. Phys. Chem. Solids*, Pergamon Press, 1957, Vol. 1, pp. 249–261.
 36. E.H. Perea, E.E. Mendez and C.G. Fonstad, "Electroreflectance of indium gallium arsenide phosphide lattice matched to indium phosphide", *Appl. Phys. Lett.* Vol. 36, No. 12 pp 978 – 980 June 1980.
 37. J.C. Hensel and G. Feher, "Cyclotron resonance experiments in uniaxially stressed silicon: Valence band inverse mass parameters and deformation potentials", *Phys. Rev.*, Vol. 129, No. 3, pp 1041–1062, Feb. 1963.
 38. E.I. Gordon, "Mode selection in GaAs injection lasers resulting from Fresnel reflection", *IEEE J. Quantum Electron*, Vol. QE–9, No.7, pp.

772–776, July 1973.

39. G.P. Agrawal and N.K. Dutta, *Long-wavelength semiconductor lasers*, Van Nostrand Reinhold, New York 1986.
40. Y.C. Chen and J.M. Liu, "Polarization bistability in semiconductor lasers", *Appl. Phys. Lett.*, Vol. 46, No. 1, pp. 16–18, Jan. 1985.
41. G. Ropars, A. Le Floch, G. Jezequel, R. Le Naour, Y.C. Chen and J.M. Liu, "The Inhibition Mechanism in Polarization Bistable Semiconductor Lasers", *IEEE J. Quantum Electron.*, Vol. 23, No. 6, pp. 1027–1031, June 1987.
42. W. Nakwaski, "Dynamical thermal properties of stripe geometry laser diodes", *IEE Proceedings*, Vol. 131 Pt. I, No. 3, pp. 941–101, June 1984.
43. L.V. Keldysh, O.V. Konstantinov and V.I. Perel, "Polarization effects in the interband absorption of light in semiconductors subjected to a strong electric field", *Sov. Phys.—Semicond.*, Vol. 3, No. 7, pp. 876–884, Jan 1970.